Preparation of Low-Valence Metal Oxide Monoliths with Three-Dimensionally Interconnected Macropores

XUANMING LU

Contents

General Introduction ---------- 1

Chapter 1 Magnesium Oxide ---------- 14

Chapter 2 Zinc Oxide ---------- 30

Chapter 3 Manganese, Cobalt, and Copper Oxides ---------- 47

Summary ---------- 70

List of Publications ---------- 72

Acknowledgement ---------- 74

General Introduction

On December 29th, 1959, Richard Feynman set a stage for nanoscience research through his famous speech entitled “There’s Plenty of Room at the Bottom”. After that, a large number of traditional bulk materials have been reformed into those with smaller size. As well recognized by scientists today, we have a noun: *nanomaterial*, defined a matter with at least one dimension sized from 1 to 100 nanometers. Thanks to their small sizes in nanomaterials, some of them not only show better performance than the traditional one, but also present new properties which do not be found in the bulk one. Abundant nanomaterials have been prepared by various kinds of methods, and characterized on the performance of optical, electrical, magnetic, catalytic, medical properties.

The industrialization and commercialization of nanomaterials, however, evolve much slowly compared with the progress in academia. Costs of raw materials and preparation, large-scale production, stability and recyclability may be the critical problems for the practical application. Among them, the aggregation of nanomaterials occurring in the processes of their assembly, use, recycle will deteriorate their performance since they become no more “nano”. In order to solve the problem of aggregation, many researchers prepare the nanomaterials into the forms of core-shell, fiber, film, foam, and those on favorable supports. Aerogel is one of the most famous form in foam, which has a three-dimensionally (3D) interconnected structure self-supported by nano-particles and thus possesses a high specific surface area [1]. The aerogel has abundant micropores ($d_{\text{pore}} < 2$ nm) and mesopores ($d_{\text{pore}} = 2 \sim 50$ nm), which can supply huge amounts of activity sites, but it lacks macropores ($d_{\text{pore}} > 50$ nm) for reactants to more easily arrive at the internal activity sites.

Over the years much attention has been paid to the synthesis of materials with hierarchically porous structure [2]. Among all the methods to prepare hierarchically porous materials, sol–gel process accompanied by spinodal decomposition has proven its advantages, such as facile method, no template, precise structural control, good reproducibility, and availableness for various kinds of materials [3]. The mechanism of this method is described as spatial arresting of the transient state

in the process of phase separation by gelation. The 3D interconnected macropore can be controlled basically by the volume fractions of gel-rich/solvent-rich phases and the gelation timing (Figure 1). The open nanopore in the gels phase is tailored by aging and drying of the networks formed by polymerization. The induction of phase separation by polymerization reaction is well explained by the Flory–Huggins theory [4, 5], whereas the spinodal decomposition as a transient (non-equilibrium) process of phase separation has been studied by Cahn [6, 7].

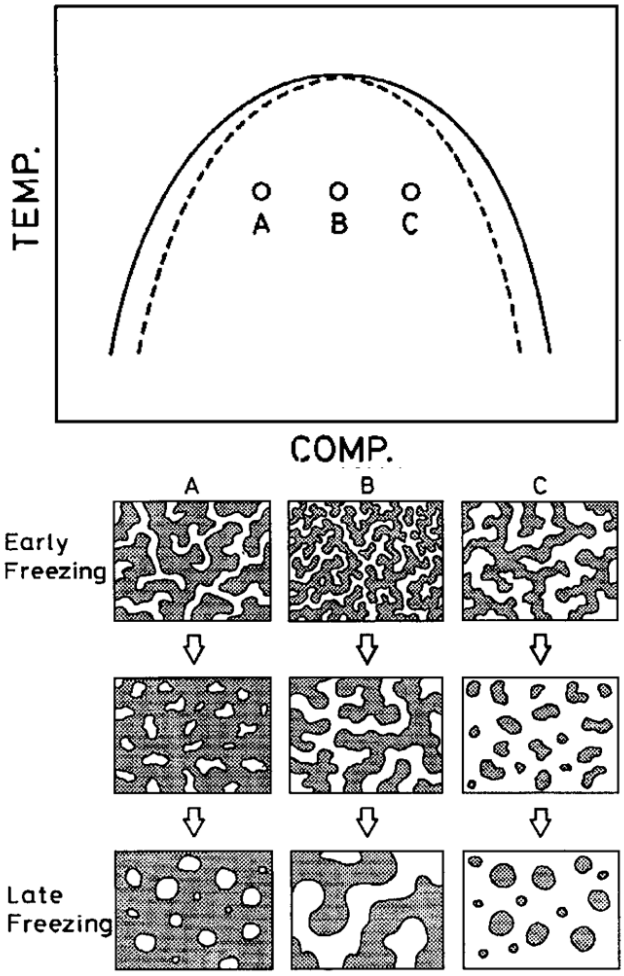

Figure 1 Various possible structures in the controls of the respective volume fractions of gel-rich/solvent-rich phases and gelation timing [8].

The hierarchically porous monolith with 3D interconnected macropores and open nanopores (abbreviated as *HP monolith* for convenience) was first prepared successfully via sol–gel process

accompanied by phase separation in silica [8]. Hereafter, numerous efforts have been made to prepare other kinds of materials into HP monoliths, such as metal oxide or phosphate, carbon, polymer, and metal organic framework (MOF). The details are summarized in Table 1.

Table 1 Summary of typical HP monoliths prepared via sol–gel process accompanied by phase separation.

Materials	Additives	Composition in HP monolith	Reference
Silica	PEO	Amorphous	9
Titania	H_2O	Rutile/Anatase TiO_2	10
	PEO	Rutile/Anatase TiO_2	11
Alumina	PEO	α-Al_2O_3/γ-Al_2O_3	12
Zirconia	PEO	Monoclinic/Tetragonal ZrO_2	13
Tin oxide	PPG	Rutile SnO_2	unpublished
Fe-based	PAAm	Fe_3O_4/Fe_3C	14
	PEO	α-Fe_2O_3	15
Ni-based	HPAA	Ni, C	16
	PEO	NiO/Ni	unpublished
Cr-based	HPAA	(Cr_2O_3, organic)/CrN/Cr_3C_2	17
Cu-based	PAAm	Cu, C	18
Niobium oxide	PTMG	T-Nb_2O_5/TT-Nb_2O_5	unpublished
Calcium phosphate	HPAA	HAP, β-TCP	19
Lithium iron phosphate	PEO, PVP	$LeFePO_4$/($LeFePO_4$, C)	20

Aluminum phosphate	PEO	Tridymite $AlPO_4$	21
Zirconium phosphate	PAAm, PEO	$Zr_2O(PO_4)_2$	22
Titan phosphate	PEO, PVP	Amorphous	23
Niobium phosphate	PAAm, PEO	Amorphous	24
Organic polymer	PDMS	PDVB	25
Metal organic frameworks	PPG	UiO-66-NH_2	26

Abbreviations: PEO: poly(ethylene oxide); PPG: polypropylene glycol; PAAm: polyacrylamide; HPAA: poly(acrylic acid); PTMG: poly(tetramethylene glycol); HAP: hydroxyapatite; TCP: tri-calcium phosphate; PVP: polyvinylpyrrolidone; PDMS: poly(dimethylsiloxane); PDVB: poly(divinylbenzene).

Let us pay attention to basic metal oxides. After the success in silica, Nakanishi and his co-workers tried to prepare other (metal) oxide HP monoliths. This epical development is presented in the Figure 2. TiO_2 and ZrO_2 HP monoliths were prepared by Konishi *et al*. in 2006 and 2008, respectively, using corresponding metal alkoxides as precursors [10, 13]. Mainly due to the difficulty in controlling the reactivity of metal alkoxides, this branch was not developed anymore. In 2007, Tokudome and his co-workers combined the epoxide-mediated method, which was developed by Gash *et al*. [27], and phase separation to prepare Al_2O_3 HP monolith from an inorganic metal salt, $AlCl_3$ (Node 1, Figure 2) [12]. In the epoxide-mediated method, epoxide acts as an acid scavenger raising the solution pH homogenously through an irreversible ring-opening reaction. The undesired precipitation thus can be avoided in a few of aqueous metal solutions (but not all). Based on the combination of epoxide-mediated method and phase separation, TiO_2, ZrO_2, and SnO_2 HP monoliths were subsequently prepared using respective inorganic salts as precursors [28, 29].

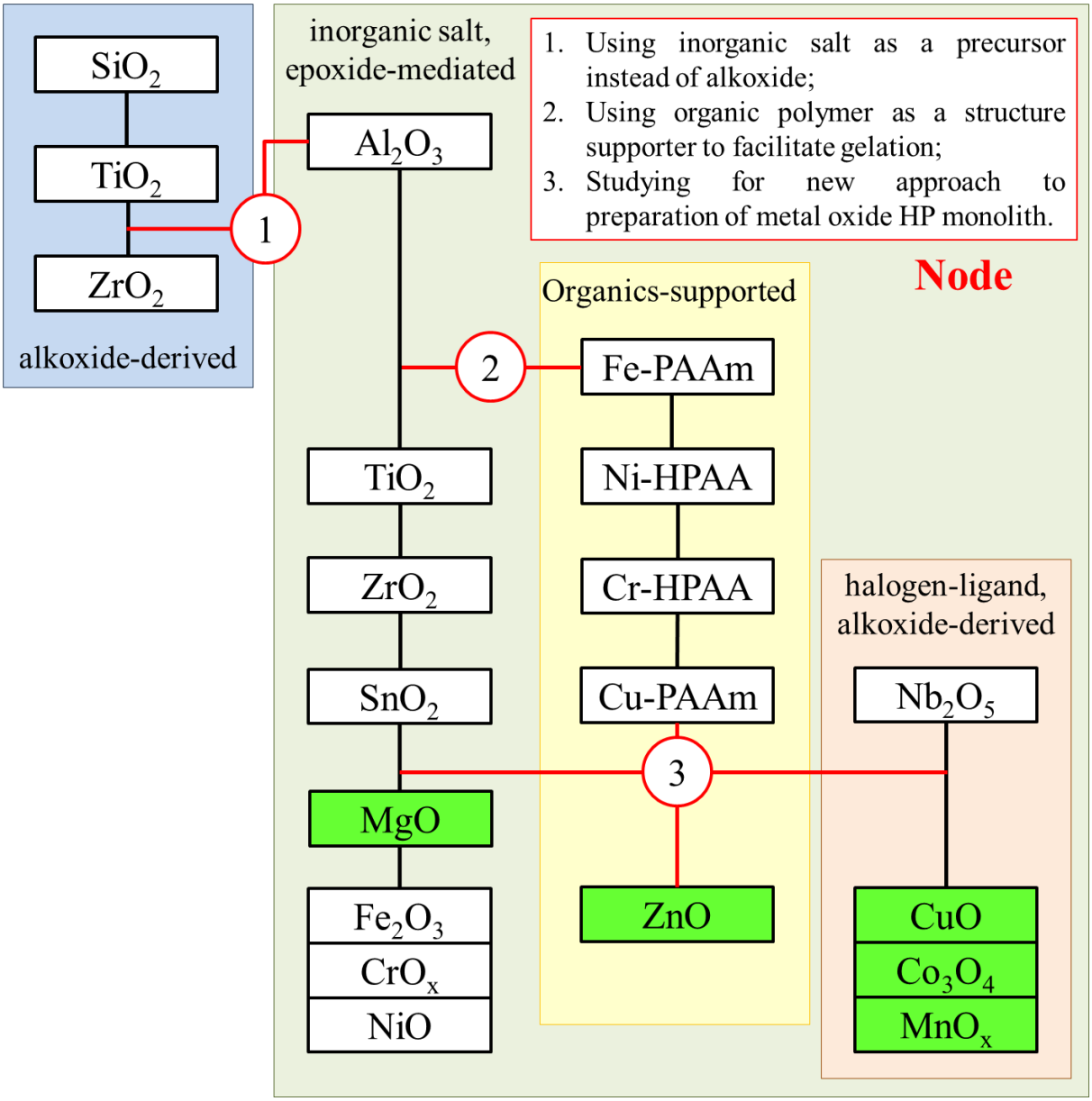

Figure 2 Development of metal oxide based HP monoliths in Nakanishi group.

Although many metal oxide aerogels had been prepared by Gash and his co-workers from the solutions of their respective metal ions (Cr^{3+}, Fe^{3+}, Ga^{3+}, In^{3+}, Zr^{4+}, Hf^{4+}, Ta^{5+}, Nb^{5+}, and W^{6+}) [30], the success of Al_2O_3 HP monolith could not be copied in the Fe_2O_3 HP monolith initially where only precipitation was obtained. It is because high concentration of metal salt is needed in preparation of HP monolith, which leads to precipitation. Consequently, an organic polymer, PAAm, which has a strong hydrogen-bonding interaction with hydrolyzed/polycondensed

metal-species, was utilized in Fe-system [14]. The PAAm not only prevents the precipitation and thus facilitates the gelation, but also induces the phase separation. Therefore, a new branch was developed (Node 2, Figure 2). Besides PAAm, another organic polymer, HPAA, had proven its feasibility. In this branch, the HP monoliths can easily be prepared from metal ions which have poor tendency to form homogeneous monolithic gels, including Ni^{2+}, Cu^{2+} [16, 18]. In the HP monoliths prepared by PAAm and HPAA, however, the monolithic form and the 3D interconnected macroporous structure can hardly be preserved after heat-treatment under oxidative conditions. This kind of HP monoliths should be termed as metal-polymer-based HP monolith, because the gel-phase structure is mainly built up by interaction between organic polymer and metal-based species. The skeleton in these HP monoliths are constructed by C−C (carbon−carbon) and metal−organic bondings rather than M−O−M (metal-oxide-metal) bondings. As a consequence, the only way to obtain crystalline metal oxide with preserved 3D interconnected macropores is heat treatment under inert atmosphere, in which the fine carbon moieties will remain in the monolith.

As will be described in Chapter 1, the present research started from the preparation of magnesium-based HP monolith. Based on the previous work, HPAA was used at first, and the Mg-HPAA-based HP monolith was obtained with ease. Certainly, the same problem was met as in the other systems using PAAm or HPAA. Obviously an alternative approach was required to prepare metal oxide HP monoliths, in which the monolithic form and macroporous structure can be preserved after heat-treatment in air for crystallization of metal oxides. Starting with MgO monolith, the author's main interest has remained in the preparation of low-valence metal oxide HP monoliths without inclusions since 2016 (Node 3, Figure 2). Five kinds of metal (Mg, Zn, Cu, Co, Mn, marked with green in Figure 2) oxide monoliths derived from corresponding divalent inorganic metal salts have been prepared in the present thesis. Three different approaches were taken, reflecting the author's ideas and understandings deepened through the experimental research.

As a basis of the research overviews, it is necessary to introduce the sol–gel process briefly at first. The most thoroughly studied example in sol–gel science is silicon tetraethoxide (or tetraethoxysilane, TEOS), $Si(OC_2H_5)_4$. The sol–gel transition of TEOS solution is caused by two

kinds of reactions: hydrolysis and polycondensation. The overall reactions for TEOS are expressed by following equations:

$$\begin{aligned} &\equiv Si-OR + H_2O \longrightarrow \equiv Si-OH + ROH \\ &\equiv Si-OH + \equiv Si-OR \longrightarrow \equiv Si-O-Si\equiv + ROH \\ &\equiv Si-OH + \equiv Si-OH \longrightarrow \equiv Si-O-Si\equiv + H_2O \end{aligned} \quad (1)$$

Since the TEOS has four alkoxide groups that can easily form four Si–O bonds to construct a random 3D network via hydrolysis and polycondensation. These processes in other metal alkoxides are very similar, except for the reactivity and stereochemistry. Most metal alkoxides have higher reactivity toward water than silicon alkoxide. For example, the hydrolysis rate of $Ti(OR)_4$ is about 10^5 times faster that of $Si(OR)_4$ with the same alkoxide groups due to the low electronegativity of Ti. In the case of alkoxide of lower-valence metals which have lower electronegativity than Ti (Table 2), the reactivity thus becomes much higher. The rapid hydrolysis and polycondensation tend to cause locally dispersed polycondensed products, *i.e.* precipitations, rather than homogenous gelation with infinite network. As a result, preparations of bulk metal oxide gels and HP monoliths from alkoxides are relatively difficult.

Table 2 Electronegativity (χ_i) of metal cations with coordination number (CN) of 4 or 6 [a]

Cation	χ_i	Cation	χ_i
Si^{4+} (CN=4)	2.245	Mg^{2+}	1.234
Al^{3+}	1.513	Mn^{2+}	1.263
Ti^{4+}	1.730	Co^{2+}	1.321
Cr^{3+}	1.587	Cu^{2+}	1.372
Fe^{3+}	1.556	Zn^{2+}	1.336
Ni^{2+}	1.367		
Zr^{4+} (CN=4)	1.743		
Nb^{5+}	1.862		

[a] χ_i is calculated from eq. $\chi_i = 0.105n^* (I_m/R)^{1/2}/r_i + 0.863$, where n^* is the effective principal quantum number; *R* is Rydberg constant; r_i is ionic radii [31].

Another kind of precursor used to prepare metal oxide gels and HP monoliths is inorganic metal salt. Metal salts dissolve in aqueous solution and form aquo complexes (M–OH_2). The aquo complex can convert to hydroxo complex (M–OH) and oxo complex (M–O–M or M=O) via forced hydrolysis when the solution pH is increased. The series of equilibria is shown in Eq. 2.

$$\underset{\text{aquo}}{M-OH_2} \overset{-H^+}{\rightleftharpoons} \underset{\text{hydroxo}}{M-OH} \overset{-H^+}{\rightleftharpoons} \underset{\text{oxo}}{M=O} \qquad (2)$$

The hydrolyzed products are unstable and undergo condensation. Two kinds of condensation processes are distinguished according to the kind of bridge formed between the metal atoms: olation and oxolation. In olation process, hydroxy bridge (M–OH–M) is formed between two metal atoms and one water molecule is released (Eq. 3).

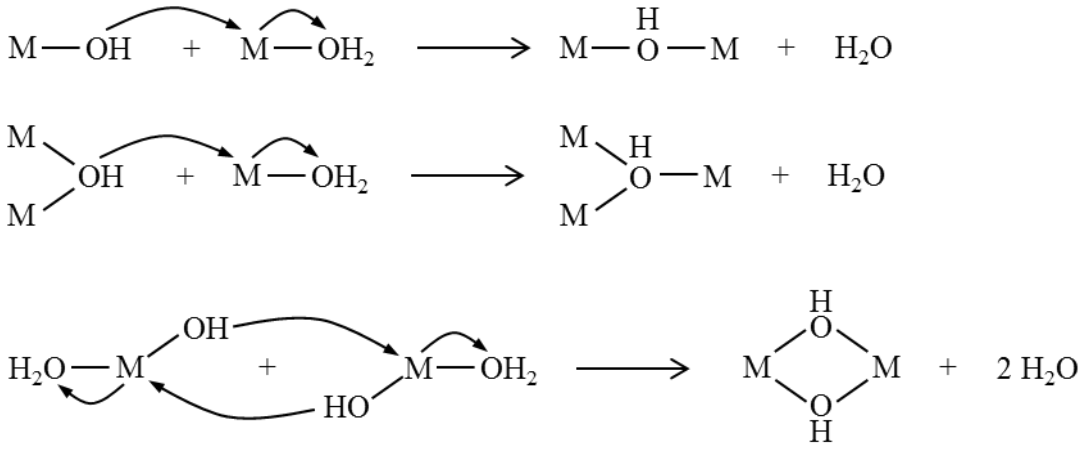

(3)

In oxolation process, oxo bridge (M–O–M) is formed and one water molecule is released (Eq. 4).

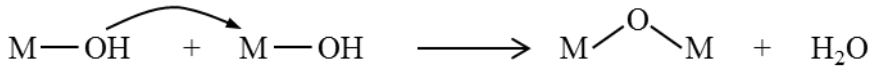

(4)

As a result, the metal oxide gels can also be prepared from inorganic metal salts in appropriate conditions.

However, preparation of a monolithic gel from metal salt, especially from the low-valence metal salt, is not an easy case as compared with that in SiO_2 system. The hydrolysis and polycondensation processes in both precursors of organic alkoxide and inorganic salt can be considered as electrophilic or nucleophilic substitution depending on the catalytic conditions. The difficulty of gelation for low-valence metal oxide can be illustrated according to the partial charge model, which was developed by Livage [32]. In SiO_2 system, the Si–O bond exhibits comparable ionicity and covalency, leaving relatively small positive partial charge on silicon atom and relatively small negative partial charge on oxygen. This leads to the low reactivity of silicon alkoxides toward both acid and base catalyzed hydrolysis/polycondensation (compared with other metals listed in Table 2). As a result, the hydrolysis and polycondensation are controllable. In other metal systems, the electron density distribution will be further concentrated toward oxygen, due to

the lower electronegativity of metal. Thus the metal and oxygen carry larger partial positive and negative charges, respectively. As a result, the metal precursors generally have high rates of hydrolysis and polycondensation. The formation of dispersed metal hydroxide precipitate dominates rather than that of extended metal oxide network.

The synthesis of MgO HP monolith will be introduced in Chapter 1. Herein, magnesium chloride hexahydrate was used as the magnesium source, and propylene oxide was used as an acid scavenger to raise the solution pH homogenously. The $Mg(OH)_2$ precipitate is easily produced when the solution pH is increased. In order to suppress the aggregation and growth of $Mg(OH)_2$ particles, PVP and 1,3,5-benzenetricarboxylic acid (H_3BTC) were employed. Due to the moderate hydrogen-bonding interaction with Mg-species, the monolithic form and 3D interconnected macroporous structure can be preserved after removal of the PVP by heat treatment in air. On the other hand, H_3BTC was found to be effective in suppressing the oriented growth of the micrometer-sized crystalline phase. Although the structural collapse after heat treatment in air, which usually happens in other organic-supported systems, could be avoided, the MgO HP monolith was still fragile. That is because the main bonds in the MgO-system can be considered as hydroxy bridge (M–OH–M) and oxo bridge (M–O–M) in primary/secondary particles and relatively weak hydrogen bonding (M–OH…O–M) between secondary crystalline aggregates.

In Chapter 2, zinc oxide with 3D interconnected macropores was prepared using citric acid (CA) as a structure supporter. In ZnO-system, the phase-separated morphology could be controlled by the ratio of methanol to epoxides in the starting solution without using any organic polymer. The Zn-CA gel was heat-treated in air with the purpose of removing the organic moieties and crystallizing the ZnO, finally resulting in ZnO monolith with 3D interconnected macropores and an open nanoscale network. Compared with the systems using organic polymers, PAAm and HPAA as structure supporters, the use of small molecule as a structure supporter, to some extent, can avoid the structural collapse after heat treatment in air. The heat-treated ZnO monolith, however, is fragile, because the skeleton in the as-dried gel sample is not fully composed of M–O–M bonds.

From the previous works, it can be found that any as-dried gel constructed by organic supporting

components will become fragile after removal of the organic moieties by heat treatment in air. In order to prepare a rigid crystalline metal oxide HP monolith, the polycondensation between metal species themselves to form a non-oriented M–O–M network is most essential. According to the partial charge model discussed above, the hydrolysis and polycondensation can be controlled by the charge distributions around the metal and oxygen atoms. Therefore, the hydrolysis and polycondensation can be facilitated by modifying the electron densities around metal and oxygen atoms. In Chapter 3, the highly electronegative atoms, bromine atoms were introduced adjacent to the central metal ions to overcome the difficulty of gelation for Mn^{2+}, Co^{2+}, and Cu^{2+}. The brominated metal alkoxides ($MBr_x(OR)_y$) with Br ligands and OR groups were produced in the incomplete reaction between epichlorohydrin and metal bromides. Then the diluted hydrochloric acid was added to trigger the hydrolysis and polycondensation. Due to the presence of the Br ligand, the partial positive/negative charges around metal/oxygen, respective, are decreased. As a result, the hydrolysis and polycondensation become controllable. A monolithic gel constructed with M–O–M network can be prepared successfully by this method. The crystalline oxide monoliths with 3D interconnected macroporous structures were obtained after heat treatment in air. Although there are still rooms to be improved, it can be claimed that the method presented in this thesis provides a novel route to prepare gels containing low-valence (less electronegative) metal elements in the form of HP monoliths.

Reference

[1] S. S. Kistler, *Nature* **1931**, *127*, 741.

[2] X. Yang, L. Chen, Y. Li, J.C. Rooke, C. Sanchez, B. Su, *Chem. Soc. Rev*. **2017**, *46*, 481.

[3] K. Nakanishi, *J Porous Mater.* **1997**, *4*, 67.

[4] P. J. Flory, *J. Chem. Phys.* **1942**, *10*, 51.

[5] M. L. Huggins, *J. Am. Chem. Soc.* **1942**, *64*, 2716.

[6] J. W. Cahn, *Acta Mater*. **1961**, *9*, 795.

[7] J. W. Cahn, *J. Chem. Phys*. **1965**, *42*, 93

[8] K. Nakanishi, N. Soga, *J. Am. Cerm. Soc.* **1991**, *74*, 2518.

[9] K. Nakanishi, N. Soga, *Bull. Chem. Soc. Jpn*. **1997**, *70*, 587.

[10] J. Konishi, K. Fujita, K. Nakanishi, K. Hirao, *Chem. Mater.* **2006**, *18*, 6069.

[11] G. Hasegawa, K. Kanamori, K. Nakanishi, T. Hanada, *J. Am. Ceram. Soc.* **2010**, *93*, 3110.

[12] Y. Tokudome, K. Fujita, K. Nakanishi, K. Miura, K. Hirao, *Chem. Mater.* **2007**, *19*, 3393.

[13] J. Konishi, K. Fujita, S. Oiwa, K. Nakanishi, K. Hirao, *Chem. Mater.* **2008**, *20*, 2165.

[14] Y. Kido, K. Nakanishi, A. Miyasaka, K. Kanamori, *Chem. Mater.* **2012**, *24*, 2071.

[15] Y. Hara, K. Kanamori, K. Morisao, R. Miyamoto, K. Nakanishi, *J. Mater. Chem. A* **2018**, *6*, 9041.

[16] Y. Kido, K. Nakanishi, N. Okumura, K. Kanamori, *Micropor. Mesopor. Mat.* **2013**, *176*, 64.

[17] Y. Kido, G. Hasegawa, K. Kanamori, K. Nakanishi, *J. Mater. Chem. A* **2014**, *2*, 745.

[18] S. Fukumoto, K. Nakanishi, K. Kanamori, *New J. Chem*. **2015**, *39*, 6771.

[19] Y. Tokudome, A. Miyasaka, K. Nakanishi, T. Hanada, *J. Sol–gel Sci. Technol.* **2011**, *57*, 269.

[20] G. Hasegawa, Y. Ishihara, K. Kanamori, K. Miyazaki, Y. Yamada, K. Nakanishi, T. Abe, *Chem. Mater.* **2011**, *23*, 5208.

[21] W. Li, Y. Zhu, X. Guo, K. Nakanishi, K. Kanamori, H. Yang, *Sci. Technol. Adv. Mater.* **2013**, *14*, 045007.

[22] Y. Zhu, T. Shimizu, T. Kitajima, K. Morisato, N. Moitra, B. Nicolas, T. Kiyomura, K. Kanamori, K. Takeda, H. Kurata, M. Tafu, K. Nakanishi, *New J. Chem.* **2015**, *39*, 2444.

[23] Y. Zhu, K. Yoneda, K. Kanamori, K. Takeda, T. Kiyomura, H. Kurata, K. Nakanishi, *New J. Chem.* **2016**, *40*, 4153.

[24] D. Gao, B. Zhao, H. Liu, K. Morisato, K. Kanamori, Z. He, M. Zeng, H. Wu, J. Chen, K. Nakanishi, *Catal. Sci. Technol.* **2018**, *8*, 3675.

[25] J. Hasegawa, K. Kanamori, K. Nakanishi, T. Hanada, S. Yamago, *Macromolecules* **2009**, *42*, 1270.

[26] Y. Hara, K. Kanamori, K. Nakanishi, *Angew. Chem. Int. Ed.* 10.1002/anie.201911499.

[27] A. E. Gash, T.M. Tillotson, J. H. Satcher Jr., J.F. Poco, L.W. Hrubesh, R.L. Simpson, *Chem. Mater*. **2001**, *13*, 999.

[28] W. Li, X. Guo, Y. Zhu, Y. Hui, K. Kanamori, K. Nakanishi, *J. Sol–gel Sci. Technol.* **2013**, *67*, 639.

[29] X. Guo, J. Song, Y. Lvlin, K. Nakanishi, K. Kanamori, H. Yang, *Sci. Technol. Adv. Mater.* **2015**, *16*, 025003.

[30] B. J. Clapsaddle, D. W. Sprehn, A. E. Gash, J. H. Satcher Jr., R. L. Simpson, *J. Non-cryst. Solids* **2004**, *350*, 173.

[31] K. Li, D. Xue, *J. Phys. Chem. A* **2006**, *110*, 11332.

[32] J. Livage, M. Henry, C. Sanchez, *Prog. Solid St. Chem.* **1988**, *18*, 259.

Chapter 1

Magnesium Oxide

1.1 Introduction

Hierarchically porous materials have been attracting keen attentions in the fields of energy conversion and storage [1], catalysis [2], separation [3], and adsorption [4]. The multiscale porous materials possess well-defined pores in discrete length-scales typically ranging from micro- (< 2 nm), meso- (2 ~ 50 nm) to macro-pores (> 50 nm). The interconnected macropores provide the materials with high permeability, while the open mesopores and micropores contribute to enlarge the available surface area. Hierarchically porous monolith integrating these properties offers advantages of recyclability, ease of separation, which are in general unavoidable problems with nanoparticles.

One of the commonly used methods to prepare hierarchically porous monoliths is the so-called sol–gel process accompanied by phase separation. The sol–gel process offers advantages of broad applicable chemical compositions, mild reaction conditions, and versatility in preparing materials in various sizes and shapes. Nearly 30 years ago, Nakanishi and Soga successfully synthesized hierarchically porous silica, SiO_2, monolith via sol–gel process accompanied by phase separation [5]. In this method, macropores are formed via polymerization-induced phase separation, which is commonly recognized in organic polymer blends and multicomponent inorganic glasses. The driving force of phase separation can be qualitatively explained by the Flory–Huggins equation [6, 7]. The sol–gel process proceeds simultaneously with the phase separation, and then freezes its transient structure including the co-continuous structure, which consists of two conjugate phases (solid gel-phase and fluidic sol-phase). The monolith with three-dimensionally (3D)

interconnected solid skeletons and macropores can be obtained after a removal of the solvent-phase by washing and drying.

Based on the silica system, many hierarchically porous metal oxide monoliths have been successfully synthesized, such as titanium dioxide, TiO_2 [8, 9], zirconium dioxide, ZrO_2 [10], aluminum oxide, Al_2O_3 [11]. In the former two cases, a relatively high concentration of alkoxide precursors had to be employed to produce crack-free monoliths. Since the reactivity of alkoxides of titanium or zirconium is much higher than that of silicon alkoxide [12], it is necessary to suppress the reactivity of the alkoxides by an addition of chelating agents [9] or by a careful control of solution pH [10] for a successful preparation of the oxide monoliths.

In 2001, Gash and his co-workers used inorganic metal salts, instead of alkoxides, as precursors to synthesize iron (III) oxide [13] and aluminum oxide monoliths [14] in the form of supercritically dried aerogel. Epoxide as an acid scavenger was added to the precursor solution to increase the solution pH homogeneously, which drove the hydrolysis and polymerization of hydrated metal species to allow homogeneous gelation. Tokudome and his co-workers introduced the polymerization-induced phase separation method to the abovementioned epoxide-mediated sol–gel system to produce hierarchically porous Al_2O_3 monoliths. Hierarchically porous iron-based [15], nickel-based [16], chromium-based [17], and copper-based [18] monoliths have also been synthesized through similar processes. In these cases, unlike Al_2O_3 monolith, the monolithic forms were not preserved after calcination under oxidative conditions. Due to the strong hydrogen-bond interaction between the metal (oxy)hydroxide oligomers and the phase-separation inducers such as polyacrylamide, PAAm and poly(acrylic acid), HPAA, the solid gel-phase obtained contains an appreciable fraction of organic components and only sparsely crosslinked inorganic components. Heat treatment under reducing atmosphere is an only way to preserve monolithicity and macroporous structure in the resultant calcined gels with fine carbon inclusions.

It is therefore still a challenge to prepare a single-phase crystalline metal oxide monolith with hierarchical pores via sol–gel process accompanied by phase separation. Furthermore, it is more difficult for divalent metal ions to form monolithic oxides without the aid of structure-supporting components. Since the acidities of $[M(H_2O)_x]^{2+}$ complexes are much lower than those for metal

aquo complexes with higher valence, the protonation of the added epoxide and resultant increase in pH of the solution will be suppressed. It may tend to lead to precipitation rather than homogeneous gelation [16, 19].

In the present work, the preparation of magnesium oxide, MgO, monolith with a 3D interconnected macroporous structure via sol–gel process accompanied by phase separation has been studied. Polyvinylpyrrolidone, PVP, was used as a phase separation controller to control the phase-separated morphology. Unlike the HPAA- or PAAm-containing systems, PVP was found not to be a main component to mechanically support the monolithic form due to the relatively weak interaction with metal hydroxide, and has a weak effect on preventing Mg^{2+} aquo complexes from condensation compared to HPAA or PAAm. As a result, the degree of polycondensation in the Mg-based species will be high enough to maintain the monolithic form after the removal of organic components. In addition, 1,3,5-benzenetricarboxylic acid, H_3BTC, was employed to suppress the growth of oligomers/particles, and to modify the meso- and micropore structures, which influenced on the specific surface area of the products. To the best of our knowledge, there is limited number of reports on the synthesis of the hierarchically porous monoliths with divalent metal oxides. The present work may provide a route to synthesize monolithic divalent metal oxides with appreciable specific surface area.

1.2 Experimental

1.2.1 Starting materials

Magnesium chloride hexahydrate ($MgCl_2 \cdot 6H_2O$, > 98 %), distilled water (H_2O), methanol (MeOH, > 99.8 %), 2-propanol (IPA, > 99 %), and *n*-hexane (> 99 %) were purchased from Kishida Chemical Co., Ltd. (Japan). 1,3,5,-benzenetricarboxylic acid (H_3BTC, > 98 %) was purchased from Tokyo Chemical Ind. Co., Ltd. (Japan). Poly(vinylpyrrolidone) (PVP, M_v = 10 000 Da) and propylene oxide (PO) were purchased from Sigma–Aldrich Japan. All the agents were used without further purification.

1.2.2 Preparation of gel samples

The typical synthesis procedure for the monolithic Mg-based gel is as follows. 2 mmol of $MgCl_2 \cdot 6H_2O$ was dissolved in an aqueous methanol solution homogeneously, followed by an addition of 0.16 g of PVP. Then the solution was heated up to 50 °C for 20 min to accelerate the dissolution of PVP. After cooling the solution down to room temperature, 0.28 mL of PO was injected into the solution under stirring, followed by stirring for 1 min. The solution was tightly sealed and placed in a constant temperature oven at 25 °C for gelation. In the case of synthesis with H_3BTC, a predetermined amount of H_3BTC was dissolved in the initial methanol solution. After gelation, the gel was aged at the same condition for 24 h. The as-dried gel was obtained after solvent exchange with IPA at 60 °C for 3 times, 12 h for each, and then drying at 40 °C for 24 h. The crystalline MgO monolith was obtained by the heat treatment in air.

1.2.3 Characterization

The structures in the micrometer range of resultant gels were examined by a scanning electron microscope (SEM; JSM-6060S, JEOL, Japan). Nitrogen adsorption–desorption isotherms were obtained using BELSORP-mini II (Bel Japan Inc. Japan). Before the measurement, samples were degassed under vacuum at 200 °C. Specific surface area was calculated using the Brunauer–Emmett–Teller (BET) method, and the pore size distribution in the mesopore regime was calculated from the adsorption branch of the isotherm using the Barrett–Joyner–Halenda (BJH) method.

Thermal evolutions of the as-dried gels were measured by a thermogravimetric-differential thermal analyzer (TG-DTA; Thermo plus EVO, TG-DTA 8120, Rigaku Co., Japan), at a heating rate of 5 °C min^{-1}, with a continuous air supply at 100 mL min^{-1}. The Fourier transform infrared (FT-IR) spectra were obtained by a FT-IR spectrometer (IRAffinity-1, Shimadzu Co., Japan) using the KBr technique. Samples were dried at 120 °C for 1 h before each FT-IR measurement. Crystal structures of the samples were investigated by an X-ray diffractometer (XRD; RINT Ultima III, Rigaku Co., Japan) using Cu Kα ($\lambda = 0.154$ nm) as an incident beam.

1.3 Results and discussion

1.3.1 Effects of solvent and polymer

Table 1.1 Results of the samples prepared with varied volume ratios of methanol to water.

$V_{methanol}/V_{water}$ (mL/mL)	Results
0.75/0	Monolithic gel
0.70/0.05	Monolithic gel
0.60/0.15	Monolithic gel
0.50/0.25	Gel-like aggregates
0.40/0.35	Gel-like aggregates
0/0.75	Sediment

While keeping the total volume of solvent mixture at 0.75 mL and the amount of PVP at 0.16 g, the morphologies of as-dried gels obtained at varied ratios of methanol to water (Table 1.1) were investigated. As shown in the SEM images as Figure 1.1, although macroscopic gelation was observed, disordered aggregates of platy crystallites with a limited fraction of micrometer-scale pores were formed in the absence of externally added water (Figure 1.1(a)). The gel-phase exhibited spherical and 3D interconnected features when prepared with the $V_{methanol}/V_{water}$ ratio of 0.70/0.05 (Figure 1.1(b)). At the ratio of 0.60/0.15, the gel-phase became more or less disordered aggregates of spherical units with increased porosity (Figure 1.1(c)), showing that the structure of resultant gel was sensitively influenced by the composition of the solvent. The gels prepared with the ratio of 0.50/0.25 and 0.40/0.35 were monolithic but even softer and more fragile than that obtained with the ratio of 0.70/0.05, and only macroscopic sediment-precipitate phases were obtained when no methanol was used.

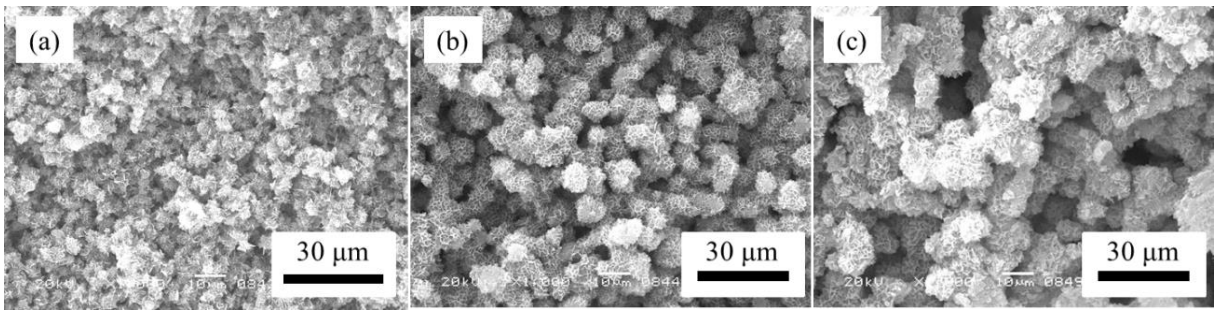

Figure 1.1 SEM images of as-dried gels prepared with varied ratios of $V_{methanol}/V_{water}$ (mL/mL): (a) 0.75/0; (b) 0.70/0.05; (c) 0.60/0.15. (PVP: 0.16 g)

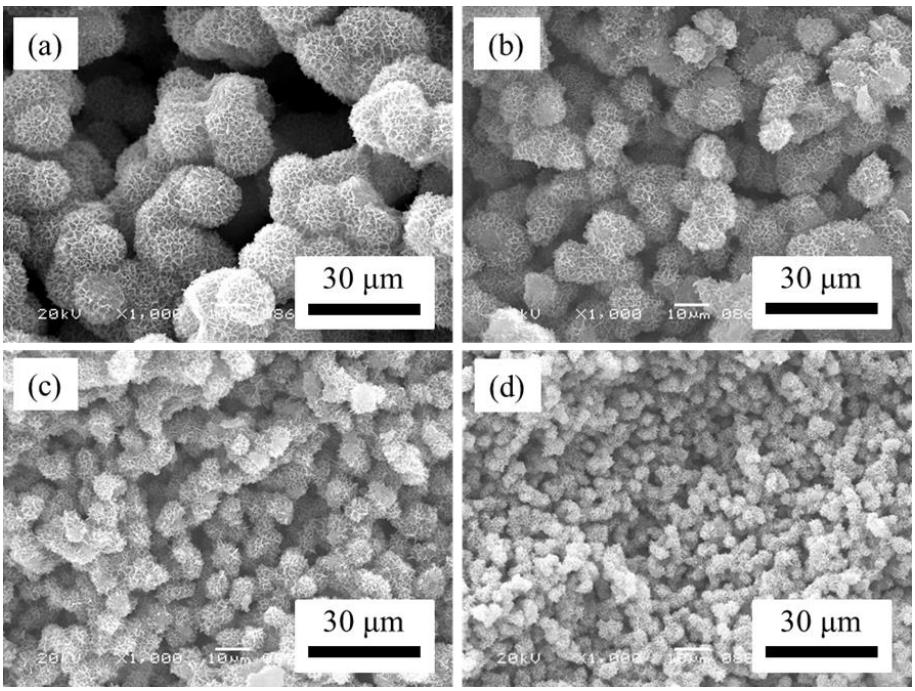

Figure 1.2 SEM images of as-dried gels prepared with varied amounts of PVP: (a) 0 g; (b) 0.08 g; (c) 0.16 g; (d) 0.24 g. ($V_{methanol}/V_{water}$: 0.70/0.05 (mL/mL))

Figure 1.2 shows the SEM images of as-dried gels synthesized with varied amounts of PVP at the $V_{methanol}/V_{water}$ ratio of 0.70/0.05. Even in the absence of PVP, spherical particles aggregated to form a monolithic gel (Figure 1.2(a)). With an increase of the amount of PVP, the size of spherical particles became smaller accompanied by the improvement in homogeneity of the macroporous structure (Figure 1.2(b)–(d)). The amount of PVP had a weak influence on the gelation time, which indicated that the PVP mainly controlled the phase separation tendency of the present gelling

system.

Divalent magnesium ions are known to exist in an aqueous solution as hexa-aquo complexes in the form of $[Mg(H_2O)_6]^{2+}$. The forced hydrolysis takes place when the pH of the solution is increased, as the equilibrium shown in Eq. 1.1.

$$[Mg-OH_2]^{2+} \rightleftharpoons [Mg-OH]^{+} + H^{+} \quad (1.1)$$

Subsequent growth via olation and crystallization into $Mg(OH)_2$ results in the formation of platy hexagons as precipitates. Due to the inherent poor solubility of $Mg(OH)_2$ in water, the essential driving force of phase separation to form the gel-phase is assumed to be the precipitation of $Mg(OH)_2$ out of the aqueous solvent. When nanocrystalline $Mg(OH)_2$, possibly loose aggregates of crystalline particles, are formed in the absence of PVP, at least a part of crystallites can grow freely to form larger platy crystalline precipitates. Since the starting hydrated chloride contains 6 moles of molecular water per Mg, it is possible, even without an external addition of water, for the precursor molecules to form complexes containing multiple hydroxo (Mg–OH) ligands. The rate of formation and aggregation of nanocrystalline $Mg(OH)_2$ rapidly increases with an increase of available water in the solvent phase. If such grown aggregates are tenuous and stay dispersed for an appreciable period of sol–gel transition, the final product will become a monolithic gel instead of dispersed or sediment aggregates.

In the present system, the platy hexagonal precipitates secondarily aggregated to form spherical gel-phase domains. It is obvious in Figure 1.2(a), in the $MgCl_2 \cdot 6H_2O$–MeOH–PO system, the formation of monolithic gels is possible without an addition of PVP. The domain sizes are decreased with increasing the amount of PVP. It indicated that the incorporation of PVP is effective in suppressing phase separation tendency. The platy habit of the primary crystalline particles, however, remains almost unchanged with additions of PVP in varied concentrations.

1.3.2 Effect of H_3BTC

Since the growth of nanocrystalline precipitates into larger platy particles leads to the decreased

specific surface area of the material, ligands that can suppress the growth of $Mg(OH)_2$ is desired to obtain materials with appreciable specific surface area. With the purpose of preserving fine crystallite size, H_3BTC was utilized, which can form coordinate bonds between its carboxy groups and Mg ions. With an increased concentration of H_3BTC, both of the length and thickness of the crystalline plates on the surface of skeleton decreased (Figure 1.3). The size of spherical aggregates increased gradually with an increase of the H_3BTC accompanied by prolonged gelation time, suggesting that the coordination of H_3BTC to Mg^{2+} ions slowed down the growth of nanocrystalline $Mg(OH)_2$ aggregates. The nanoporous structures of the samples prepared with varied concentrations of H_3BTC after heat treatment at 500 °C were characterized by nitrogen sorption measurements. The BJH pore size distributions of the samples prepared with varied amounts of H_3BTC are shown in Figure 1.4. Without H_3BTC, almost no pores were recognized in the mesopore regime. The fraction of pores larger than 30 nm increased with the increasing amount of H_3BTC, in good accordance with the fact that crystalline plates became finer. Other polycarboxylic acids, such as citric acid and tartaric acid, exhibited the similar effects.

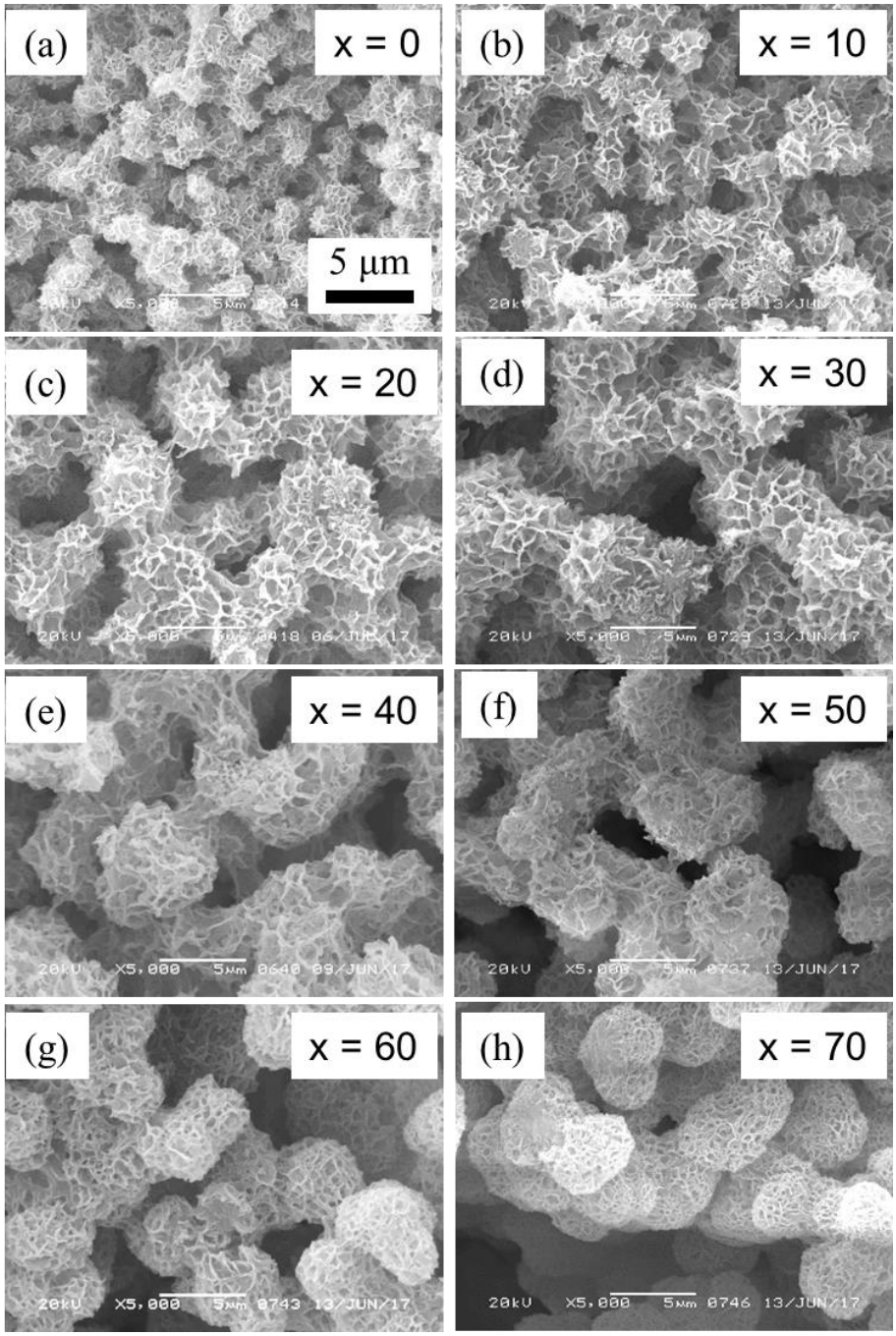

Figure 1.3 SEM images of as-dried gels prepared with x μmol of H_3BTC. ($V_{methanol}/V_{water}$: 0.70/0.05 (mL/mL); PVP: 0.16 g)

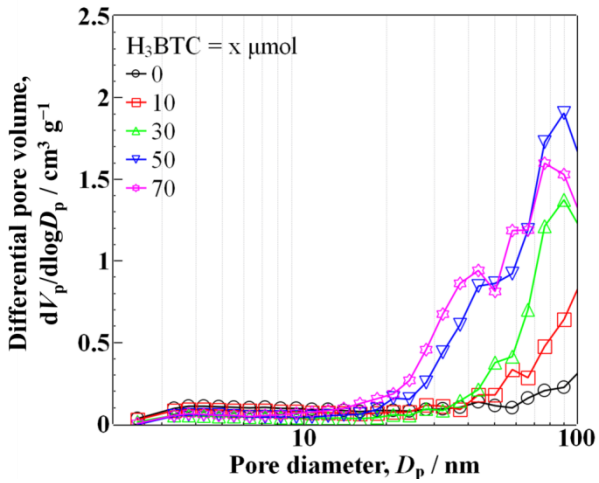

Figure 1.4 Pore size distributions of heat-treated (500 °C for 2 h) samples prepared with varied amounts of H_3BTC. ($V_{methanol}/V_{water}$: 0.70/0.05 (mL/mL); PVP: 0.16 g)

1.3.3 Compositional analysis

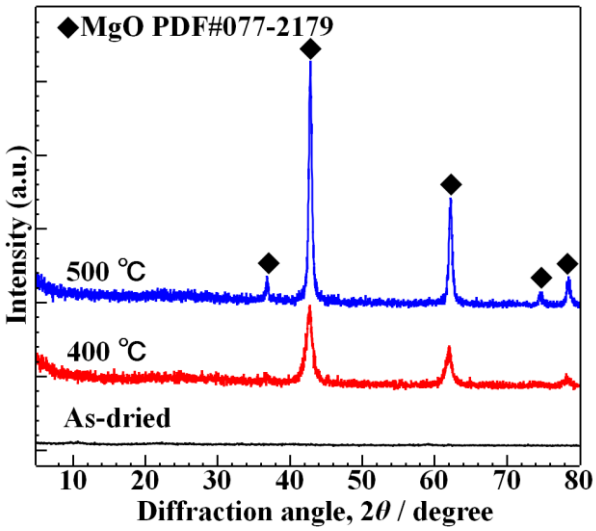

Figure 1.5 XRD patterns of as-dried sample before and after heat treatment at varied temperatures. ($V_{methanol}/V_{water}$: 0.70/0.05 (mL/mL); PVP: 0.16 g)

Figure 1.5 shows the XRD patterns of the as-dried gels before and after the heat treatment at varied temperatures. The halo pattern indicates that the as-dried gel is amorphous. The diffraction peaks became evident after heating at 400 and 500 °C. The four intense diffractions at 36.9°,

42.9°, 62.3°, and 78.6° are respectively ascribed to the (111), (200), (220) and (222) crystal planes of MgO (PDF#077-2179), periclase.

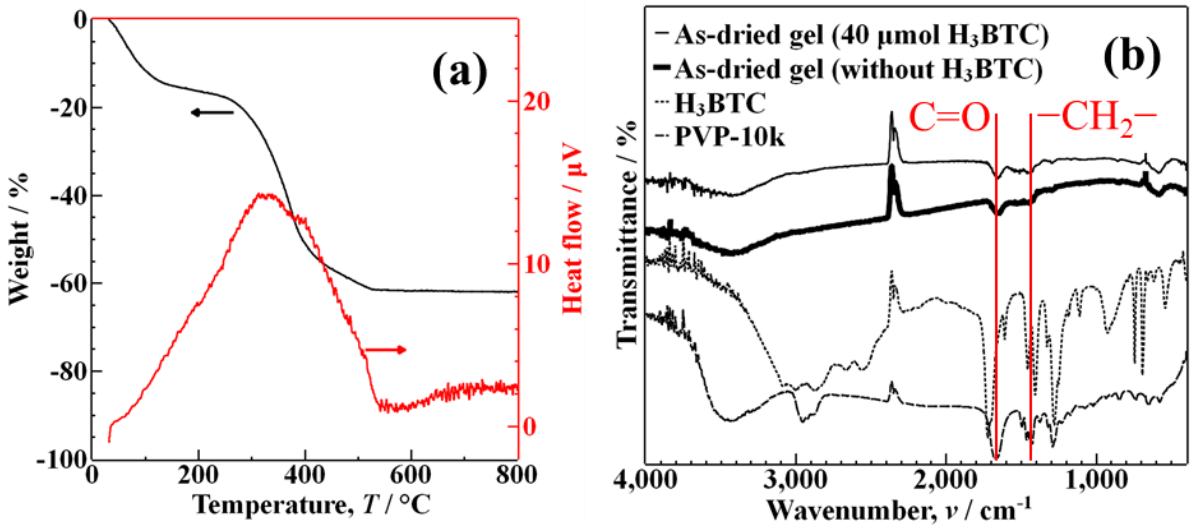

Figure 1.6 (a) TG-DTA curves of as-dried sample prepared without H_3BTC; (b) FT-IR spectra of as-dried samples prepared in the presence/absence of 40 μmol of H_3BTC. ($V_{methanol}/V_{water}$: 0.70/0.05 (mL/mL); PVP: 0.16 g)

The thermal evolutions of as-dried gel prepared without H_3BTC is illustrated in Figure 1.6(a). About 16 % of weight loss was observed at the temperature range below 200 °C, which is attributed to desorption of physically adsorbed water. The 46 % of weight loss at the temperature range from 200 to 500 °C accompanied by a broad exothermic peak is ascribed to the combustion of PVP and dehydration of hydroxyl groups. Assuming all initially added Mg atoms remained in the skeleton as MgO, there is considerable amount of PVP remained on/in the skeleton of as-dried gel. Although the mass of MgO accounts for only about 38 % of the initial solid mass of skeleton, the monoliths did not collapse after the removal of PVP by heating. The skeleton is dominantly formed by the Mg–O bonds after the heat treatment, although the mechanical strength decreased substantially.

The FT-IR spectrometer was utilized to examine the chemical structure of the as-dried gels prepared with 0.16 g of PVP and in the presence/absence of 40 μmol of H_3BTC (Figure 1.6(b)).

The presence of H_3BTC was not clearly detected by FT-IR. The adsorption bands at around 1660 and 1420 cm^{-1} are attributed to the vibrations of carbonyl group (C=O) and methylene group (–CH_2–), respectively, indicating that PVP is present on/in the skeleton, which agrees with the result of TG-DTA. The band attributed to the vibration of carbonyl group in the gel samples showed only a slight shift from that of the free carbonyl group (from 1666 to 1653 cm^{-1}), indicating that the interaction between PVP and the Mg-based particles is relatively weak [20]. Considering the fact that the samples remained monolithic even after the removal of PVP by heat treatment, being different from the cases with PAAm and HPAA, PVP does not work as the main component to mechanically support the Mg-based network.

1.3.4 Drying process and heat treatment

Drying of wet gels by evaporation of the liquid in the pores exerts capillary forces that may cause the collapse of micropores, mesopores and even macropores. Three different processes were examined to remove solvents from the wet Mg-based monoliths: 1. solvent exchange with IPA and drying at 40 °C; 2. solvent exchange with *n*-hexane and drying at 40 °C; 3. supercritical drying (SCD) after exchange with IPA and supercritical CO_2 in a pressure chamber. Supercritical drying is considered to be the way that the porous structure of the gel can be preserved to the highest extent.

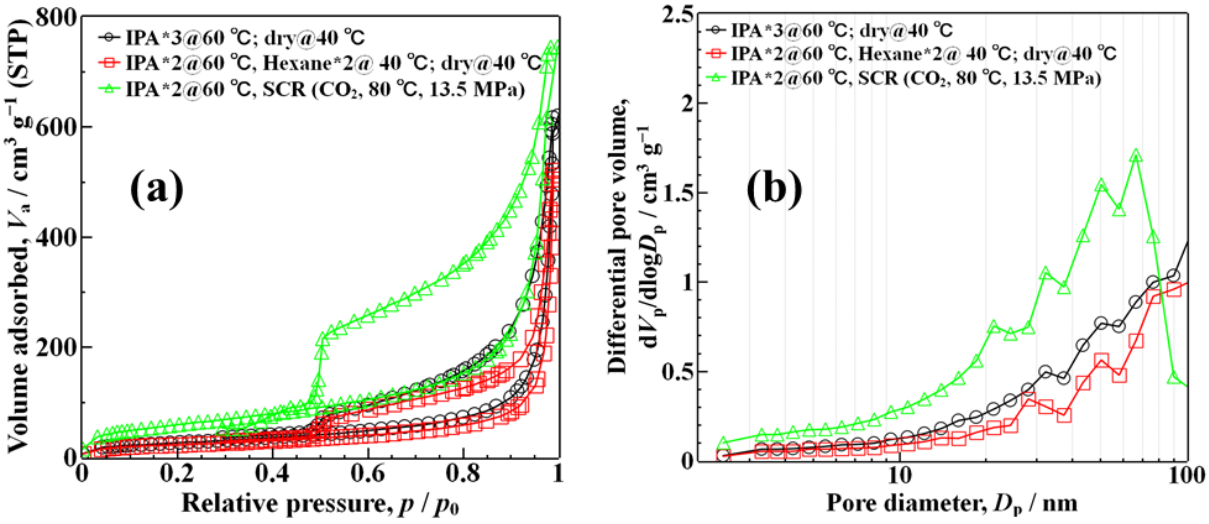

Figure 1.7 N_2 adsorption desorption isotherms (a) and pore size distributions (b) of samples

prepared by varied drying processes. ($V_{methanol}/V_{water}$: 0.70/0.05 (mL/mL); PVP: 0.16 g; H_3BTC: 20 μmol)

Figure 1.7(a) and 1.7(b) respectively show the nitrogen adsorption−desorption isotherms and the corresponding pore size distributions of the samples prepared with 20 μmol of H_3BTC and dried by the different processes 1 to 3 described above. All the samples exhibit the isotherms of type IV of the IUPAC classification with relatively small uptakes at lower relative pressures. The hysteresis loops of type H3 indicates that the pores are formed as interstices of plate-like particles, which agrees with the SEM results. Figure 1.7(b) shows that considerable fractions of micropores and mesopores have collapsed in the samples dried in ambient conditions at 40 °C relative to that dried by supercritical drying. The BET surface area also shows the values consistent with this result (Table 1.2).

The samples ambient-dried with IPA were used to examine the heat evolution of the nanostructure. It is confirmed from SEM images that the macroporous structures were not damaged after the heat treatment in air at varied temperatures (Figure 1.8). However, the shrinkage became noticeable heat-treated at 500 and 600 °C. Since $Mg(OH)_2$ is known to release water on transforming to MgO at around 350 °C, some fraction of the weight loss observed in TG-DTA above 300 °C can be ascribed to the dehydration. About 46 % weight loss in the temperature range between 200 and 500 °C well explains the shrinkage also due to the oxidative decomposition of organic components. Table 1.2 displays the summary of specific surface area and pore volume of the samples. When the sample was heated to 400 °C, the crystalline structure changed from amorphous to periclase, and most of the organics were removed. These two facts resulted in the increase in specific surface area and pore volume. With a further increase of the heating temperature, the organics were decomposed completely, and the fine MgO crystals grew further, resulting in the decreased specific surface area and pore volume of the MgO monoliths.

Table 1.2 Properties of samples obtained from varied drying processes and heat treatment temperatures. ($V_{methanol}/V_{water}$: 0.70/0.05 (mL/mL); PVP: 0.16 g; H_3BTC: 20 μmol)

Sample	BET specific surface area ($m^2\ g^{-1}$)	BJH Pore volume ($cm^3\ g^{-1}$)
As-dried (SCD)	218	1.07
As-dried (n-hexane)	82	0.79
As-dried (IPA)	96	0.91
Heat-treated (400 °C)	185	1.97
Heat-treated (500 °C)	64	0.97
Heat-treated (600 °C)	48	0.75

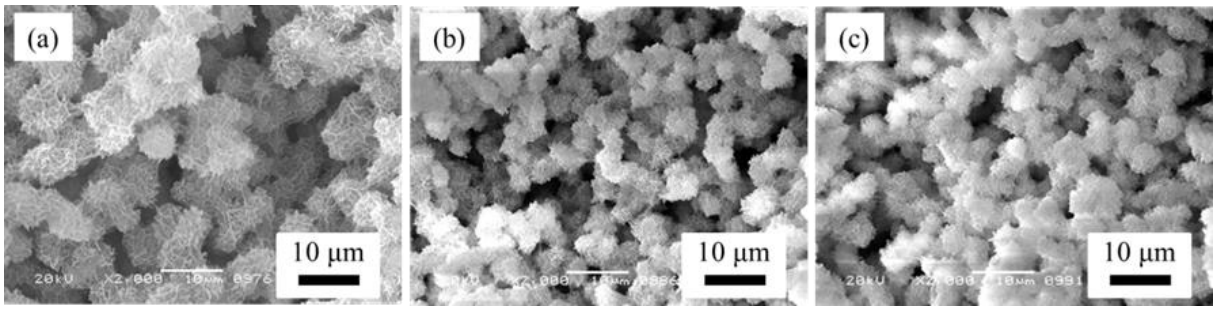

Figure 1.8 SEM images of samples after heat treatment at (a) 400, (b) 500, (c) 600 °C. ($V_{methanol}/V_{water}$: 0.70/0.05 (mL/mL); PVP: 0.16 g; H_3BTC: 20 μmol)

1.4 Conclusion

Hierarchically porous MgO monoliths with a well-defined interconnected macroporous structure have been prepared via the sol–gel process accompanied by phase separation. The macroporous structure can be controlled by the ratio of methanol to water and the amount of PVP. PVP acts as a phase separation controller suppresses the excessive phase separation tendency. After the heat treatment in air, the macroporous structure was preserved without serious damage. A polycarboxylic acid, H_3BTC, was employed to hinder the growth of precipitated crystalline particles.

The addition of H_3BTC leads to the increase of specific surface area of the monoliths. This study suggests a possible way to synthesize monolithic divalent metal oxides with high specific surface area.

References

[1] L. Shi, Z. Chu, Y. Liu, W. Jin, N. Xu, *Adv. Funct. Mater*. **2014**, *24*, 7032.

[2] G. Collins, M. Blomker, M. Osiak, J. D. Holmes, M. Bredol, C. O'Dwyer, *Chem. Mater.* **2013**, *25*, 4312.

[3] N. Tanaka, H. Nagayama, H. Kobayashi, T. Ikegami, K. Hosoya, N. Ishizuka, D. Lubda, *J. Sep. Sci*. **2000**, *23*, 111.

[4] G. Srinivas, V. Krungleviciute, Z. Guo, T. Yildirim, *Energy Environ. Sci*. **2014**, *7*, 335.

[5] K. Nakanishi, N. Soga, *J. Am. Ceram. Soc.* **1991**, *74*, 2518.

[6] P. J. Flory, *J. Chem. Phys.* **1942**, *10*, 51.

[7] M. L. Huggins, *J. Phys. Chem.* **1942**, *46*, 151.

[8] J. Konishi, K. Fujita, K. Nakanishi, K. Hirao, *Chem. Mater.* **2006**, *18*, 6069.

[9] G. Hasegawa, K. Kanamori, K. Nakanishi, T. Hanada, *J. Am. Ceram. Soc.* **2010**, *93*, 3110.

[10] J. Konishi, K. Fujita, S. Oiwa, K. Nakanishi, K. Hirao, *Chem. Mater.* **2008**, *20*, 2165.

[11] Y. Tokudome, K. Fujita, K. Nakanishi, K. Miura, K. Hirao, *Chem. Mater.* **2007**, *19*, 3393.

[12] U. Schubert, N. Hüsing, Synthesis of inorganic materials. CPI Group Ltd, Croydon, **2012**.

[13] A. E. Gash, T. M. Tillotson, J. H. Satcher Jr., J. F. Poco, L. W. Hrubesh, R. L. Simpson, *Chem. Mater*. **2001**, *13*, 999.

[14] T. F. Baumann, A .E. Gash, S. C. Chinn, A. M. Sawvel, R. S. Maxwell, J. H. Satcher Jr., *Chem. Mater*. **2005**, *17*, 395.

[15] Y. Kido, K. Nakanishi, A. Miyasaka, K. Kanamori, *Chem. Mater.* **2012**, *24*, 2071.

[16] Y. Kido, K. Nakanishi, N. Okumura, K. Kanamori, *Micropor. Mesopor. Mat.* **2013**, *176*, 64.

[17] Y. Kido, G. Hasegawa, K. Kanamori, K. Nakanishi, *J. Mater. Chem. A*, **2014**, *2*, 745.

[18] S. Fukumoto, K. Nakanishi, K. Kanamori, *New J. Chem*. **2015**, *39*, 6771.

[19] A. E. Gash, J. H. Satcher Jr., R. L. Simpson, *J. Non-Cryst. Solids* **2004**, *350*,145.

[20] M. Liu, X. Yan, H. Liu, W. Yu, *React. Funct. Polym*. **2000**, *44*, 55.

Chapter 2

Zinc Oxide

2.1 Introduction

Metal oxides (MOs) have been utilized by human beings for a long time in their history. Many kinds of MOs in modern technology play indispensable roles in the fields of catalyst, energy, environment, and so on. However, as the natural abundance is in general limited for major useful elements, functional materials have been developed in the direction of reducing the amount of raw materials required per device. With the progress of in depth understanding of the structure–property relationship, MOs have been designed from traditional bulk form into those with new structures to improve their existing performances or render them new properties [1–4]. For porous materials, efforts have been made to improve the efficiency of accommodating external substance to be interacted with active sites embedded in the materials. Multiscale porous structure is a good example, in which the nm-scale pores contribute to enlarge the available surface area, while the μm-scale pores provide the materials with high accessibility to such an active surface.

Recently, the synthesis of MOs with multiscale porosities has been abundantly reported [5–7]. Among them, the structure with three-dimensionally (3D) interconnected macropores (in μm-scale) and open nanoscale network has been realized successfully in several kinds of MOs through sol–gel method accompanied by phase separation [8–11]. Sol–gel method has been considered as a "bottom-up" approach to obtain a continuous solid network with nanopores by forced hydrolysis and polycondensation of hydrated metal cations. The interconnected macropores in μm-scale can be obtained by controlling two competitive processes, sol–gel transition and phase separation, without using any templates which physically leave unoccupied space in the resultant structure.

However, there is limited number of report on successful preparation of low-valence metal oxides based on this strategy. The main reason is that the hydrolysis and polycondensation are too rapid for low-valent metal cations due to their low electronegativities [12, 13]. The rapid hydrolysis and polycondensation tend to lead to precipitation rather than homogeneous gelation. Nevertheless, in our previous studies, Ni-based and Cu-based materials with 3D interconnected macroporous structure had been prepared using poly(acrylic acid) (HPAA) and polyacrylamide (PAAm), respectively, as structure supporters [14, 15]. Since the organic components account for predominant fraction in the skeleton, the crystallization of these oxides without losing their network structure required heat-treatment in a reducing atmosphere. As a result, considerable amount of carbon remains in the network, and then pure metal oxides with 3D interconnected macroporous structure could not be obtained.

Among the divalent MOs, zinc oxide (ZnO) has attracted a great deal of attention, scientifically and technologically, owing to its direct wide band gap of 3.37 eV. It has been extensively studied and applied in the fields of piezoelectric device [16], photocatalyst [17], gas sensor [18], transparent electrode [19], and UV photodetector [20, 21]. ZnO nanorods [22], nanowires [20, 22], nanosheets [18, 23], and nanotetrapods [21] have been abundantly synthesized, where the majority of materials shapes are classified into one- or two-dimensions except for nanotetrapods.

Some researchers tried to synthesize ZnO with 3D interconnected porous structure by a templating method [24, 25]. However, there are still a limited number of reports on synthesis of ZnO with 3D interconnected network structure, not to mention preparation without template. Nasiri and his co-workers synthesized ZnO nanoparticle networks by liquid-fed spray flame synthesis and aerosol deposition [26]. Wang and his co-workers synthesized 3D porous ZnO foam structures by a rapid combustion of ethylene glycol solution of zinc nitrate [18]. In these two works, the pores were produced by a large quantity of gases generated in the combustion process, making controls over pore structure and reproducible synthesis very difficult. Dilger and his co-workers prepared ZnO with multiple porosities by ultrafast temperature gradient chemical gas-phase synthesis [27]. In their work, an uncommon organic precursor, methylzinc methoxyethoxide was employed, and the process required a sophisticated gas phase reactor. Unlike high-valence metal oxides, such as TiO_2,

ZrO_2, and Fe_2O_3, ZnO exhibits difficulty to construct a well-defined 3D interconnected structure because of rapid crystallization of ZnO and $Zn(OH)_2$ in an aqueous solvent [21, 23]. This is one of the reasons why the preceding reports are mostly limited to low dimensional structures. It is, therefore, still a challenge to prepare pure zinc oxide with 3D interconnected network structure.

In this work, we present a facile method to synthesize 3D interconnected macroporous ZnO through sol–gel process accompanied by phase separation, and subsequent heat-treatment. The difficulty of gelation can be overcome by adopting tri-carboxylic acid, citric acid (CA), as ligands to bridge between Zn-based species [28, 29]. Propylene oxide (PO), as an acid scavenger was used to raise the solution pH homogeneously by a ring-opening reaction, which allowed gelation. On the other hand, PO as a poor solvent was distributed to the solvent phase against Zn-CA species rich phase in the phase-separation process. The size of macropores could be controlled by the concentration of PO in the starting solvents. In contrast to the cases of Ni-HPAA-system and Cu-PAAm-system mentioned above, after heat-treatment in air, the resultant gels gave crystalline metal oxide without losing their 3D interconnected network structures.

2.2 Experimental

2.2.1 Starting materials

Zinc nitrate hexahydrate ($Zn(NO_3)_2 \cdot 6H_2O$, > 98 %), citric acid (CA), propylene oxide (PO), and 1,2-epoxybutane (EB) were purchased from Sigma–Aldrich Japan. Methanol (MeOH, > 99 %), and 2-propanol (IPA, > 99 %), were purchased from Kishida Chemical Co., Ltd. (Japan). All the agents were used without further purification.

2.2.2 Preparation of Zn-based gels and crystalline ZnO

The typical synthesis procedure for the monolithic Zn-based gel is as follows. 2 mmol of $Zn(NO_3)_2 \cdot 6H_2O$ were dissolved in a predetermined amount of MeOH in a 9 mL glass bottle. Then 1 mmol of CA was added to the zinc nitrate solution under stirring. The solution was cooled in an

ice-water bath after the citric acid was dissolved completely. A predetermined amount of PO was injected into the solution in the ice-water bath under stirring, followed by stirring for 10 sec. The mixed solution was tightly sealed and placed in a refrigerator at 4 ~ 5 °C for gelation. A white opaque resultant gel was kept in the refrigerator for 30 min and subsequently aged at 25 °C for 24 h. After solvent exchange with IPA at 60 °C for 3 times, the gel was dried in a container covered by a lid with small holes at 40 °C.

The crystalline ZnO with 3D interconnected macropores was obtained by heat-treatment in air. The samples were heated, firstly, from room temperature to 300 °C with the heating rate of 1 °C min^{-1} and kept at 300 °C for 2 h. Secondly, the samples were slowly heated from 300 to 310 °C with the heating rate of 0.5 °C min^{-1} and kept at 310 °C for 2 h. Thirdly, the samples were heated from 310 °C to the target temperatures (320, 360, and 400 °C) with the heating rate of 0.5 °C min^{-1} and kept at the target temperature for 2 h. Finally, the samples were cooled with the rate of 1 °C min^{-1} down to 100 °C and left at the room temperature.

2.2.3 Characterization

The structures of resultant gels in the micrometer range and the chemical compositions were examined by scanning electron microscopy equipped with energy dispersive X-ray spectroscope (SEM-EDS, JSM-6060S, JEOL, Japan). The macropore size distributions of gels were determined by a mercury porosimeter (Autopore IV 9505, Shimadzu Co., Japan). Nitrogen adsorption–desorption isotherms were obtained using BELSORP-mini II (Microtrac BEL, Japan). Before the measurements, samples were degassed under vacuum at 120 °C. Specific surface area was calculated using the Brunauer–Emmett–Teller (BET) method, and the pore size distribution in the mesopore regime was calculated from the adsorption branch of the isotherm using the Barrett–Joyner–Halenda (BJH) method.

Thermal evolutions of the as-dried gels were measured by thermogravimetric-differential thermal analyzer (TG-DTA; Thermo plus EVO, TG-DTA 8120, Rigaku Co., Japan), at a heating rate of 1 °C min^{-1}, with a continuous air supply at 100 mL min^{-1}. The Fourier transform infrared (FT-IR) spectra were obtained by an FT-IR spectrometer (IRAffinity-1, Shimadzu Co., Japan) using KBr

technique. Crystal structures of the samples were investigated by an X-ray diffractometer (XRD; RINT Ultima III, Rigaku Co., Japan) using Cu Kα (λ = 0.154 nm) as an incident beam.

2.3 Results and discussion

2.3.1 Zn-based as-dried gels

No macroscopic gelation has been observed in the absence of CA. The time of phase separation (denoted as t_{ps}) and the time of gelation (denoted as t_g) are listed in Table 2.1. Here, t_{ps} was recorded as the time when the system lost its transparency; t_g was recorded when the system lost its fluidity. With an increasing concentration of PO in the solution, t_{ps} and t_g became shorter. PO acted as acid scavengers to raise solution pH through an irreversible ring-opening reaction with nitrate ions (Eq. 2.1).

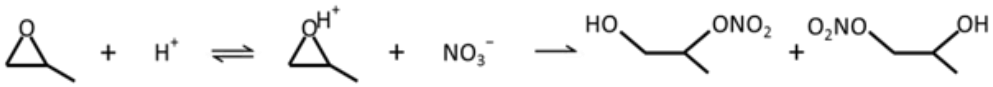

(2.1)

In the present experimental condition, higher concentration of PO simply resulted in quicker raise of the solution pH and earlier gelation. In the sample (b)–(f), the systems exhibited fluidity when they became white and opaque. Since the emergence of opaqueness can be ascribed to the onset of phase separation, the phase separation occurred earlier than gelation in these samples. Figure 2.1 shows the SEM images of as-dried gels prepared with varied volume ratios of MeOH to PO. 3D interconnected macropores are observed in all the samples except sample (a), which is a translucent gel. The size of macropores increased and the skeleton became thinner relative to the adjacent pore space with an increase of the concentration of added PO. The detailed analysis of the effects of onset of phase separation and gelation time is described in the case of pure silica in the literature [30].

Table 2.1 The phase separation time t_{ps} and gelation time t_g of samples prepared by varied ratios of MeOH to PO.

sample	MeOH/PO (mL/mL)	t_{ps} / min	t_g / min
(a)	0.8/0.6	-	130
(b)	0.7/0.7	31	50
(c)	0.6/0.8	17	30
(d)	0.5/0.9	11	15
(e)	0.4/1.0	5	10
(f)	0.3/1.1	3	6

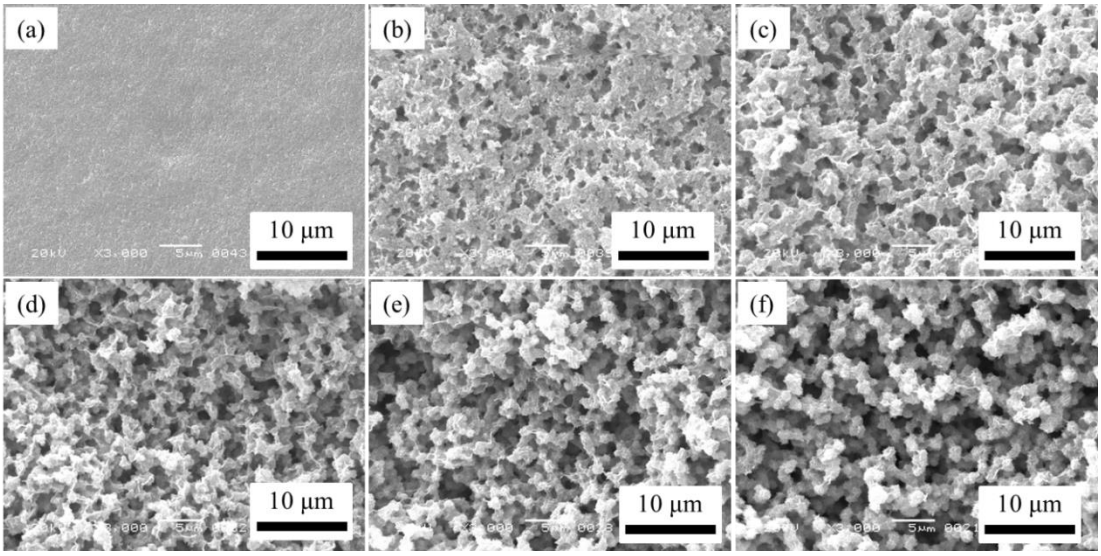

Figure 2.1 SEM images of as-dried gels prepared with varied volume ratios of MeOH to PO. (a) 0.8/0.6; (b) 0.7/0.7; (c) 0.6/0.8; (d) 0.5/0.9; (e) 0.4/1.0; (f) 0.3/1.1 (mL/mL).

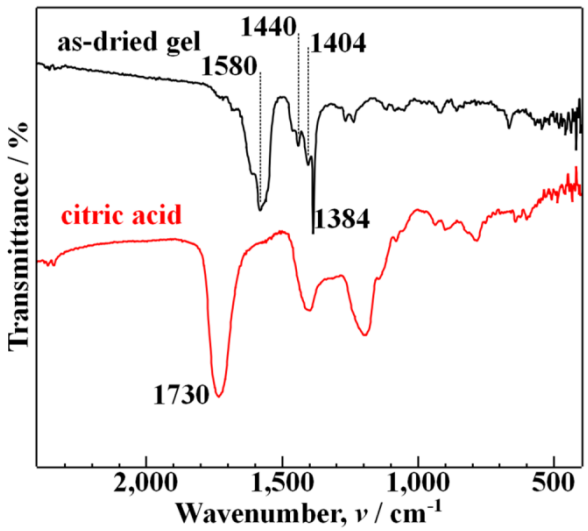

Figure 2.2 FT-IR spectra of as-dried gel (sample (c)) and citric acid.

Sample (c) was used for the examination by FT-IR spectrometer and TG-DTA. As illustrated in Figure 2.2, the sharp absorption peak at 1384 cm^{-1} in the FT-IR spectrum of as-dried gel is ascribed to nitrate ions [31–33]. The antisymmetric stretching vibrations ν_{as}(COO) appear at around 1580 cm^{-1}, whereas the corresponding symmetric stretching vibrations ν_{s}(COO) appear at 1440 and 1404 cm^{-1} [28, 32, 34]. The antisymmetric ν_{as}(COO) stretching vibration in sample (c) is shifted to lower wavenumber compared to that of free CA, indicating that the carboxy groups have coordinated to zinc cations. The wavenumber difference $\Delta\nu = \nu_{as} - \nu_{s}$ ranged from 140 to 176 cm^{-1} for sample (c) suggesting that the carboxy groups are coordinated to zinc cation in bidentate bridging mode and/or monodentate mode [29, 32–34]. In addition, the hydroxy group in the CA is also coordinated to zinc cation to form a five- and six-membered chelate ring [34, 38]. The absence of typical absorption bands corresponding to undissociated carboxylic acid groups at 1730 cm^{-1} also indicates that the majority of carboxy groups had coordinated to the zinc cations. There is no strong absorption at low wavenumber (around 500 cm^{-1}) that indicated the bonding of Zn–O–Zn is sparse in the sample [39].

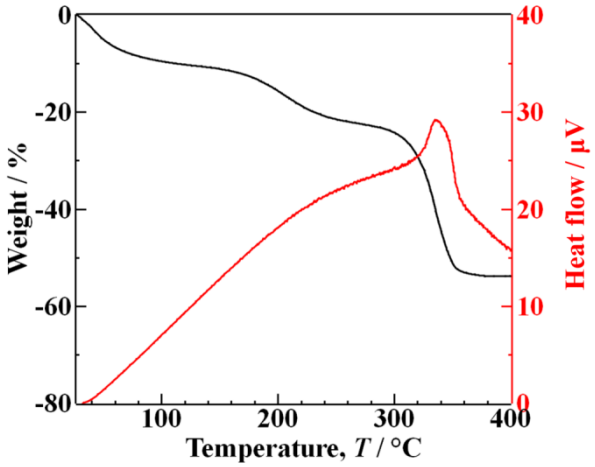

Figure 2.3 TG-DTA curves of sample (c).

According to the TG-DTA curves (Figure 2.3), about 24 % of weight loss was observed at the temperature range below 300 °C, which is attributed to dehydration of physically adsorbed water and crystalline water. About 30 % of weight loss at the temperature range from 300 to 360 °C accompanied by an exothermic peak is ascribed to the combustion of organic component. The amorphous structures transformed to wurtzite ZnO in this temperature range, which will be further discussed in the section 2.3.4.

2.3.2 Sol–gel process and phase separation

The results of FT-IR and TG-DTA indicate that the gel phase contained Zn-CA species as major components. The absence of the strong absorption band at low wavenumber in FT-IR spectrum implies that the polycondensation of Zn hydrated cation was limited. Thus the gelation is regarded as a result of the coordination of CA to zinc cation, rather than hydrolysis–condensation of zinc cation itself.

The phase separation tendency can be estimated by the Flory–Huggins equation (Eq. 2.2).

$$\Delta G \propto RT\left(\frac{\Phi_1}{P_1}\ln\Phi_1 + \frac{\Phi_2}{P_2}\ln\Phi_2 + \chi_{12}\Phi_1\Phi_2\right) \quad (2.2)$$

Where ΔG is Gibbs free energy change of mixing, R is the gas constant, T is the temperature, Φ_i and P_i are the volume fraction and the degree of polymerization of component i (i = 1 or 2), respectively, and χ_{12} is the interaction parameter, described the compatibility between component 1 and component 2. The former two terms in the bracket express the entropic contribution, and the last term expresses the enthalpic contribution. When ΔG becomes positive, the system becomes unstable, and then phase separation occurs. In the present work, the system can be simplified as a pseudobinary system, in which one is Zn-CA rich phase (denoted as component 1), and the other is the solvent-rich phase (denoted as component 2). The multiple coordination of CA to Zn cation increased P_1, while P_2 remains unity. At the same time, the preferred coordination of CA to Zn cation in place of individually hydrated species should lower the solubility of Zn-CA complex in the solvent. Consequently, the enthalpic contribution becomes more positive (repulsive). The positive enthalpic contribution will be affected by the concentration of PO in the solvent composition. Since the PO is regarded as a poor solvent against Zn-CA complex component, it is preferentially distributed to the solvent phase in the present system (as further discussed below). An increase of PO concentration thus leads to positive deviation of χ_{12}. The SEM results indicate that the enthalpic contribution became positive enough to make to the Gibbs free energy positive, at around the volume ratio of MeOH/PO = 0.7/0.7 (mL/mL), to induce the phase separation

2.3.3 Roles of methanol and propylene oxide

As the amount of MeOH was varied at a fixed amount of PO, the volume factions of solid networks and macropores only showed negligible changes (Figure 2.4). In other words, the amount of MeOH, in a limited range of MeOH/PO ratio, has a minor effect on the volume factions of gel phase (Zn-CA rich phase) and solvent phase. Thus, the MeOH can be reasonably considered as a co-solvent, which is distributed comparatively to both gel-rich phase and solvent-rich phase without markedly affecting relative volume fractions of the phases.

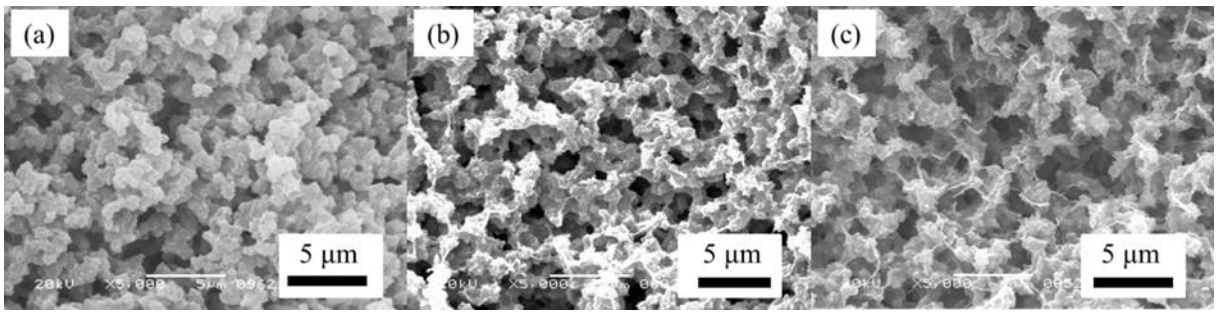

Figure 2.4 SEM images of as-dried gels prepared by varied amounts of methanol when the amount of PO was fixed at 0.9 mL. The amounts of MeOH were (a) 0.8, (b) 0.6, and (c) 0.4 mL, respectively.

In the present system, the amount of PO (8 ~ 15 mmol corresponding to 0.6 ~ 1.1 mL) is much more than the stoichiometric amount against the nitrate ion (4 mmol) in starting solution. The coordination of CA to zinc cation is dominated by the pH value. In other words, the gelation is dominated by the reaction between PO and nitric acid. In all cases, the phase separation occurred earlier than gelation (Table 2.1). It means that a considerable amount of residual PO was remained in the solution when the phase separation occurred. Therefore, PO is reasonably considered as the poor solvent. It, however, cannot exclude the possibility that the ring-opening reaction products (nitrooxypropanol) work also as a poor solvent to decrease the compatibility against Zn-CA species. The SEM images (Figure 2.1) and the mercury intrusion curves (Figure 2.5) clearly indicate the simultaneous increases in macropore volume and domain size with the concentration of PO, in reasonable agreement of the interpretation that PO works as a poor solvent against Zn-CA oligomers to promote phase separation and to increase the fraction of the solvent-rich phase.

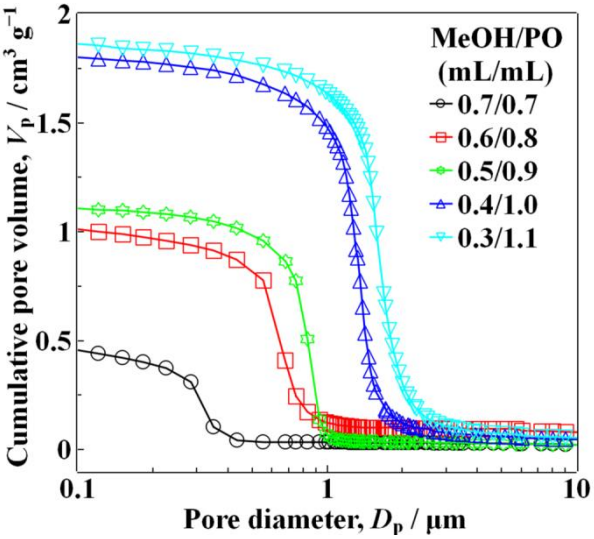

Figure 2.5 Cumulative pore volume curves of as-dried gels prepared by varied volume ratios of MeOH to PO, derived by mercury porosimetry measurement.

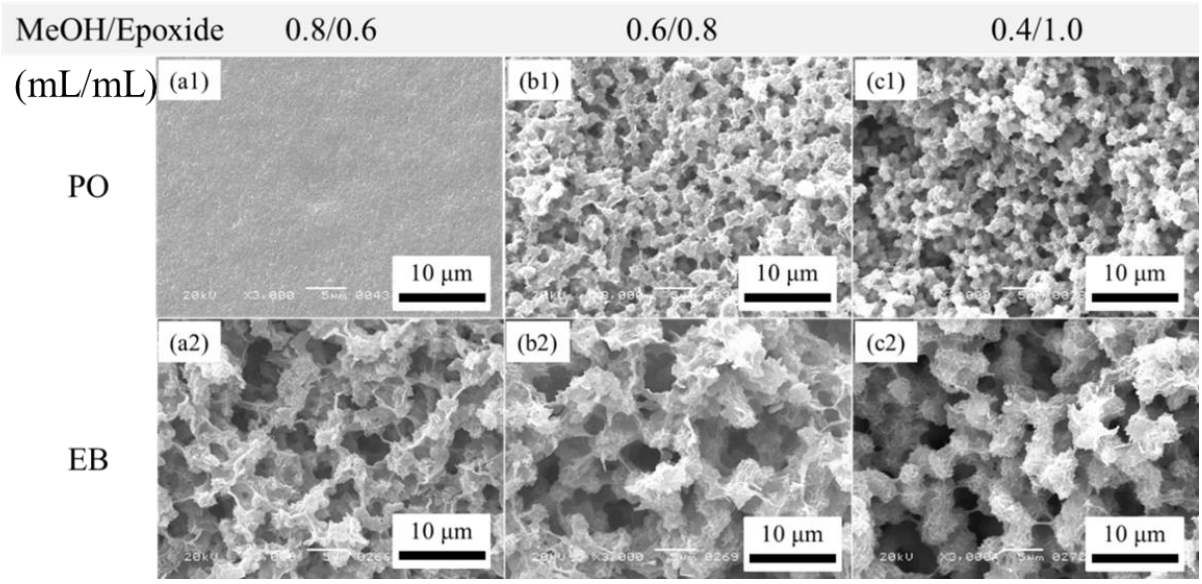

Figure 2.6 SEM images of as-dried gels prepared with PO or EB at varied amounts.

To further investigate the role of PO played in the phase separation, some samples were prepared using another epoxide, 1,2-epoxybutane (EB), keeping other conditions identical. As a result, the interconnected macroporous structure could be observed in the sample prepared by EB, but not in the sample prepared by PO, when the amounts of epoxides were 0.6 mL (Figure 2.6(a1) and 2.6(a2)). Moreover, the skeleton became coarser and interconnected macropores became larger as

well when PO was replaced with EB at the amount of 0.8 mL (Figure 2.6(b1) and 2.6(b2)) and 1.0 mL (Figure 2.6(c1) and 2.6(c2)). EB has relatively lower solubility and lower reactivity than PO in the present system. The lowered compatibility and retarded sol–gel transition are the reasons of morphologies with enhanced phase separation.

2.3.4 Crystalline ZnO with 3D interconnected macropores

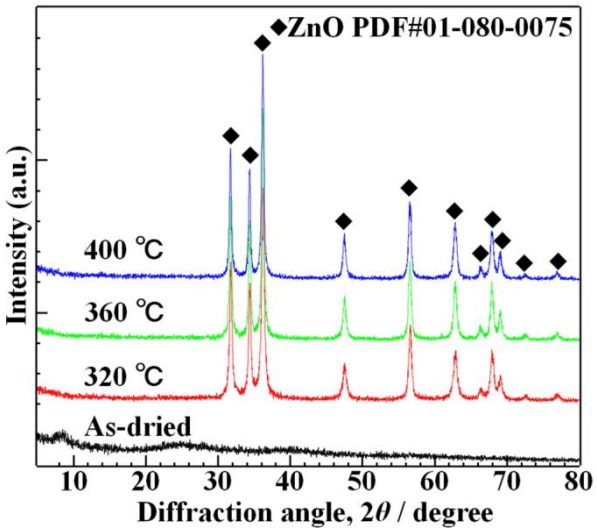

Figure 2.7 XRD patterns of sample (c) before and after heat-treated at varied temperatures.

The heat-treatment evolution was studied using sample (c) in Table 2.1. XRD patterns illustrated that wurtzite ZnO without any impurity phase could be obtained after heat-treated in air above 320 °C (Figure 2.7). The overall 3D interconnected macroporous structures were preserved after heat-treated in air, naturally accompanied by the isotropic shrinkages (Figure 2.8). The result of TG-DTA shows that the majority of organic components were removed when heat-treated above 360 °C. According to the EDS results (data not shown), about 7 wt % of carbon was detected in the sample after heat-treated at above 360 °C for 2 h. This remaining of carbon may be included in ZnO polycrystalline structure so that it is hard to be removed completely, even the heat-treatment temperature up to 500 °C. Nevertheless, it can be claimed that 3D interconnected crystalline ZnO with minor carbon inclusions could be prepared by this method. (In previous works on divalent

metal oxide based monolith, in which organic polymers with acrylamide or carboxy groups were used to support the 3D network structure, the monolithic form and macroporous structure were destroyed after heat-treatment in air.)

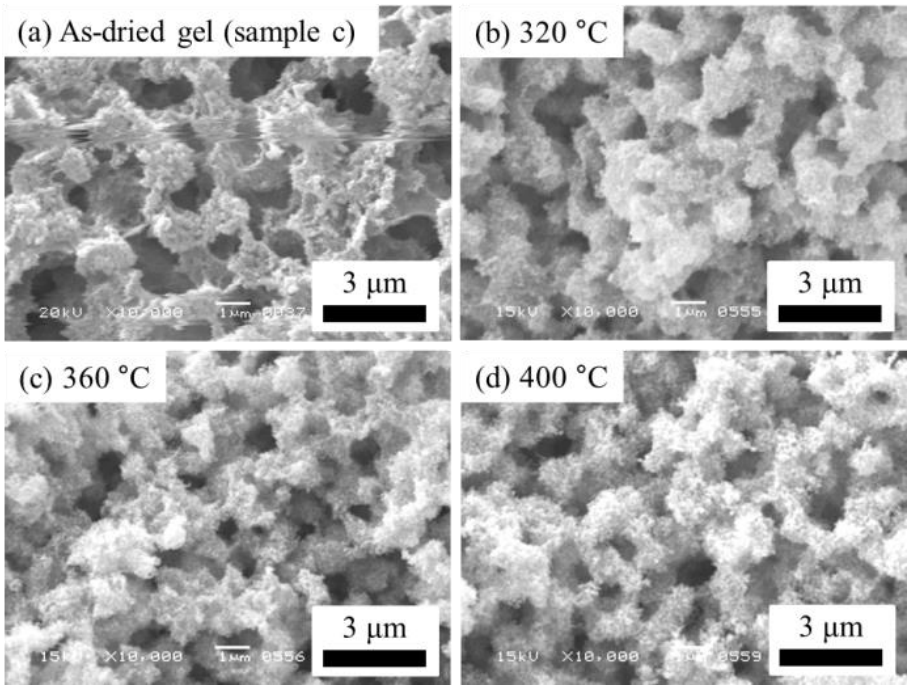

Figure 2.8 SEM images of Zn-based as-dried gel (a) before and (b)–(d) after heat-treated at varied temperatures.

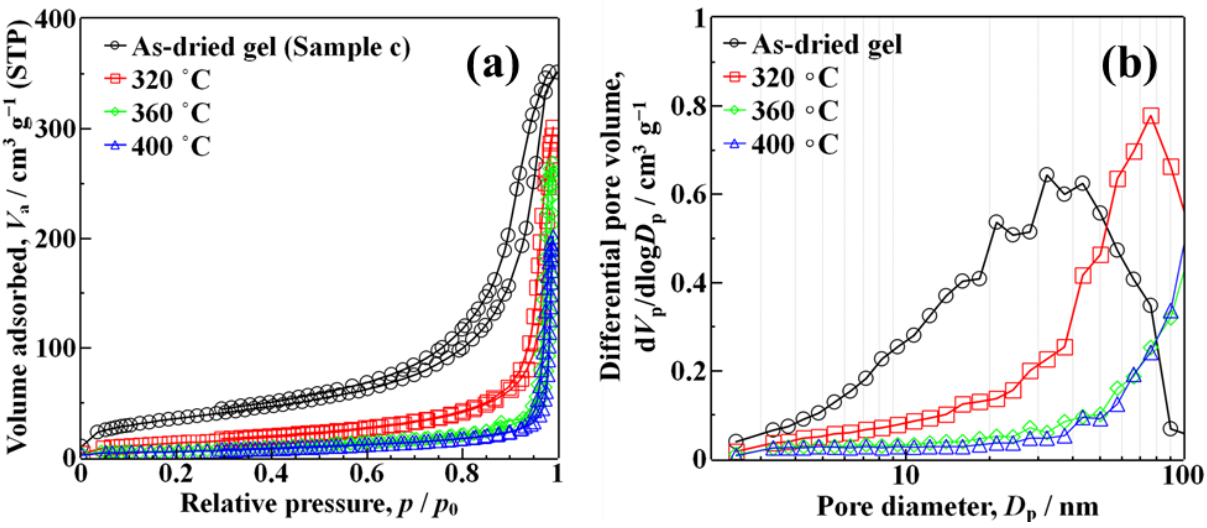

Figure 2.9 (a) Nitrogen adsorption–desorption isotherms and (b) corresponding BJH pore size distributions obtained from as-dried samples (sample (c)) before and after heat-treated at varied temperatures.

Figure 2.9(a) and 2.9(b) show the nitrogen adsorption–desorption isotherms and the corresponding pore size distributions, respectively, of the as-dried gels before and after heat-treatment at varied temperatures. All the samples exhibited the isotherms of type IV of the IUPAC classification with relatively small uptakes at lower relative pressures. It indicates that the limited volumes of micropores are present in the all ZnO samples. Figure 2.9(b) shows that the pore size distribution shifts to larger size region after the heat treatment. Moreover, the specific surface area (S_{BET}) and pore volume ($V_{p\,(BJH)}$) decreased from 50 to 18 m^2 g^{-1} and from 0.46 to 0.31 cm^3 g^{-1}, respectively, with a further increase of the heat-treated temperature from 320 to 400 °C (Table 2.2). These results are reasonably ascribed to the growth of individual ZnO nanoparticles and their interstitial spaces.

Table 2.2 BET surface area, S_{BET}, and BJH pore volume, V_p of sample (c) before and after heat-treated at varied temperatures.

sample (c)	S_{BET} / m^2 g^{-1}	$V_{p\ (BJH)}$ / cm^3 g^{-1}
As-dried	131	0.53
320 °C	50	0.46
360 °C	20	0.41
400 °C	18	0.31

2.4 Conclusions

Monolithic ZnO with 3D interconnected macroporous structure has been successfully synthesized via sol–gel process accompanied by phase separation. The difficulty of the gelation for Zn cation has been overcome by coordination with citric acid. The phase separation is induced by the coordination of CA to Zn cation. The epoxides play duplicated roles: 1. scavenging nitric acid to raise the solution pH homogeneously and then induce the coordination; 2. controlling the phase separation behavior through the solubility of Zn-CA oligomers in the mixed solvent. Epoxides (and/or the produced derivatives) are found to work as the poor solvent. Consequently, the 3D macroporous structure can be controlled by the concentrations (and kinds) of epoxides in the starting composition. To the best of our knowledge, this is the first report on the synthesis of ZnO with controllable and highly defined 3D interconnected macroporous structure without using soft- or hard-templates. This study may provide a novel route to synthesize other divalent metal oxides with 3D interconnected macropores.

References

[1] M. Zheng, H. Tang, L. Li, Q. Hu, L. Zhang, H. Xue, H. Pang, *Adv. Mater*. **2018**, *5*, 1700592.

[2] H. Tan, W. Sun, L. Wang, Q. Yan, *ChemNanoMat* **2016**, *2*, 562.

[3] G. Zhang, X. Xiao, B. Li, P. Gu, H. Xue, H. Pang, *J. Mater. Chem. A* **2017**, *5*, 8155.

[4] C. Yuan, H. Wu, Y. Xie, X. Lou, *Angew. Chem. Int. Ed*. **2014**, *53*, 1488.

[5] D. Grosso, G.J. de A.A. Soler-Illia, E.L. Crepaldi, B. Charleux, C. Sanchez, *Adv. Funct. Mater.* **2003**, *13*, 37.

[6] X. Huang, H. Yu, J. Chen, Z. Lu, R. Yazami, H. H. Hng, *Adv. Mater.* **2014**, *26*, 1296.

[7] D. Zhao, J. Qin, L. Zheng, M. Cao, *Chem. Mater.* **2016**, *28*, 4180.

[8] Y. Tokudome, K. Fujita, K. Nakanishi, K. Miura, K. Hirao, *Chem. Mater.* **2007**, *19*, 3393.

[9] J. Konishi, K. Fujita, K. Nakanishi, K. Hirao, *Chem. Mater.* **2006**, *18*, 6069.

[10] J. Konishi, K. Fujita, S. Oiwa, K. Nakanishi, K. Hirao, *Chem. Mater*. **2008**, *20*, 2165.

[11] Y. Hara, K. Kanamori, K. Morisao, R. Miyamoto, K. Nakanishi, *J. Mater. Chem. A* **2018**, *6*, 9041.

[12] U. Schubert, N. Husing, *Synthesis of Inorganic Materials*, Wiley-VCH, Weinheim, **2012**.

[13] A. E. Gash, T. M. Tillotson, J. H. Satcher, L. W. Hrubesh, R. L. Simpson, *J. Non-Cryst. Solids* **2001**, *285*, 22.

[14] Y. Kido, K. Nakanishi, N. Okumura, K. Kanamori, *Micropor. Mesopor. Mat.* **2013**, *176*, 64.

[15] S. Fukumoto, K. Nakanishi, K. Kanamori, *New J. Chem*. **2015**, *39*, 6771.

[16] Z. Wang, *Adv. Funct. Mater.* **2008**, *18*, 3553.

[17] N. Daneshvar, D. Salari, A. R. Khataee, *J. Photochem. Photobiol. A* **2004**, *162*, 317.

[18] Z. Jing, J. Zhan, *Adv. Mater*. **2008**, *20*, 4547.

[19] D. Chen, J. Liang, C. Liu, G. Saldanha, F. Zhao, K. Tong, J. Liu, Q. Pei, *Adv. Funct. Mater.* **2015**, *25*, 7512.

[20] C. Soci, A. Zhang, B. Xiang, S.A. Dayeh, D. P. R. Aplin, J. Park, X. Bao, Y. Loand, D. Wang, *Nano Lett.* **2007**, *7*, 1003.

[21] D. Gedamu, I. Paoulowicz. S. Kaps, O. Lupan, S. Wille, G. Haidarschin, Y. K. Mishra, R.

Adelung, *Adv. Mater*. **2014**, *26*, 1541.

[22] L. Vayssieres, *Adv. Mater.* **2003**, *15*, 464.

[23] J. Li, H. Fan, X. Jia, *J. Phys. Chem. C* **2010**, *114*, 14684.

[24] E. Kim, Y. Vaynzof, A. Sepe, S. Guldin, M. Scherer, P. Cunha, S. Roth, U. Steiner, *Adv. Funct. Mater.* **2014**, *24*, 863.

[25] H. Yan, Y. Yang, Z. Fu, B. Yang, L. Xia, S. Fu, F. Li, *Electrochem. Commun.* **2005**, *7*, 1117.

[26] N. Nasiri, R. Bo, F. Wang, L. Fu, A. Tricoli, *Adv. Mater*. **2015**, *27*, 4336.

[27] S. Dilger, C. Lizandara-Pueyo, M. Krumm, S. Polarz, *Adv. Mater*. **2012**, *24*, 543.

[28] M. Liang, O. Deschaume, S.V. Patwardhan, C.C. Perry, *J. Mater. Chem.* **2011**, *21*, 80.

[29] B. Chen, X. Wang, S. Zhang, C. Wei, L. Zhang, *J. Porous Mater.* **2014**, *21*, 1035.

[30] S.A.M. Lima, F.A. Sigoli, M.R. Davolos, M. Jafelicci Jr., *J. Alloys Compd.* **2002**, *334*, 280.

[31] K. Nakanishi, *J. Porous Mater*. **1997**, *4*, 67.

[32] G. Wu, L. Wang, D. G. Evans, X. Duan, *Eur. J. Inorg. Chem.* **2006**, *2006*, 3185.

[33] P. Gerstel, R. C. Hoffmann, P. Lipowsky, L. P. H. Jeurgens, J. Bill, F. Aldinger, *Chem. Mater.* **2006**, *18*, 179.

[34] D. Chen, Y. Wang, Z. Lin, F. Huang, *J. Mol. Struct.* **2010**, *966*, 59.

[35] S. Doeuff, M. Henry, C. Sanchez, J. Livage, *J. Non-Cryst. Solids* **1987**, *89*, 206.

[36] F. X. Perrin, V. Nguyen, J. L. Vernet, *J. Sol–gel Sci. Technol.* **2003**, *28*, 205.

[37] G. B. Deacon, R. J. Phillips, *Coord. Chem. Rev.* **1980**, *33*, 227.

[38] P. Che, D. Fang, D. Zhang, J. Feng, J. Wang, N. Hu, J. Meng, *J. Coord. Chem.* **2011**, *58*, 1581.

[39] S. Gago, M. Pillinger, T. M. Santos, J. Rocha, I. S. Goncalves, *Eur. J. Inorg. Chem.* **2004**, *2004*, 1389.

Chapter 3

Manganese, Cobalt, and Copper Oxides

3.1 Introduction

Hierarchically porous monolith termed “HP monolith” hereafter, with 3D interconnected macropores and open nanopores has been studied for various applications, such as separation [1–4], electrochemistry [5–9], adsorbent [10–12], catalyst [13] and support materials for catalyst/enzyme [14, 15]. One of the synthetic strategies to prepare HP monoliths is spatially arresting the transient state in the process of spinodal decomposition by gelation [16], as illustrated in Scheme 3.1. In this strategy, the 3D interconnected macropores can be obtained via phase separation, and the open nanopores are tailored by aging and drying of networks formed by the polycondensation. Several kinds of materials, including silica [1, 2, 4, 16], metal oxides [3, 12, 17–21], carbon [7–9], phosphates [5, 10, 22, 23], have been prepared successfully into HP monoliths via sol–gel process accompanied by phase separation.

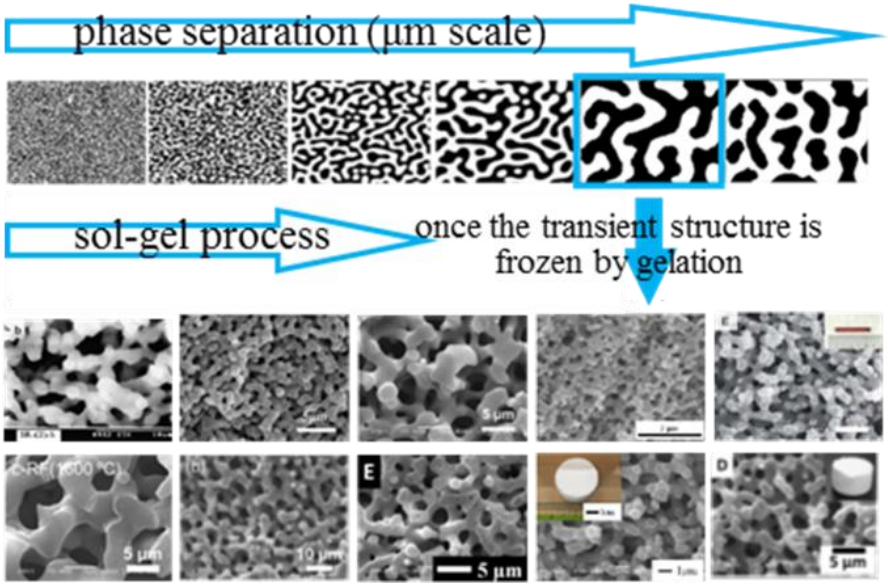

Scheme 3.1 Synthetic strategy based on sol–gel process accompanied by phase separation. From left to right, first row: SiO_2 [2]; Al_2O_3 [18]; TiO_2 [3]; ZrO_2 [19]; Fe_2O_3 [12]; second row: Carbon [7]; $LiFePO_4$ [5]; ZrP_2O_7 [10]; MgO/niobium phosphate [13]; Titanium phosphate [23].

Let us pay attention to basic metal oxide HP monoliths. According to the kind of precursor, two different strategies for preparation of oxide HP monoliths are classified. Firstly, it is using organic alkoxides (denoted as $M(OR)_x$) as precursors. The first oxide HP monolith prepared via sol–gel process accompanied by phase separation was SiO_2 HP monolith [24]. The gelation of SiO_2 derived from silicon alkoxides has been well studied in sol–gel science, thus preparation of a homogenous SiO_2 gel is easy. For obtaining 3D interconnected macropores, it is necessary to use some organic polymer, such as poly(ethylene oxide) (PEO), or to modify the solvent composition to control the phase separation [16]. Followed by the success in SiO_2, TiO_2 [25, 26] and ZrO_2 [19] HP monoliths have been prepared by this strategy. However, the metal alkoxides generally have faster hydrolysis and polycondensation rates than $Si(OR)_4$ due to the relatively higher positive partial charge on their central metal atoms. For example, the hydrolysis rate of $Ti(OR)_4$ is about 10^5 times faster than that of $Si(OR)_4$ under the same condition. Needless to say other tri-valent and di-valent metal alkoxides, which have higher reactivity than $Ti(OR)_4$. The high reactivity of many metal alkoxides toward water causes precipitation due to local quick polycondensation rather

than homogeneous gelation with spatially extended network. Thus it is necessary to suppress the high reaction rate using strong acid [19, 25] or complex agents [26] for preparation of a homogenous gel. Then the phase separation can be controlled by polymer or solvent composition, which is similar to the SiO_2-system.

Secondly, it is using inorganic metal salts as precursors. Most of reported metal oxide based monolithic gels and HP monoliths are prepared via epoxide-mediated method, which is developed by Gash and his co-workers [27]. Compared with metal alkoxides, the inorganic metal salts can be stable and cheap. In the epoxide-mediated method, epoxides act as acid scavengers raising the solution pH homogenously through the irreversible ring-opening reaction (Eq. 1. *e.g.* propylene oxide).

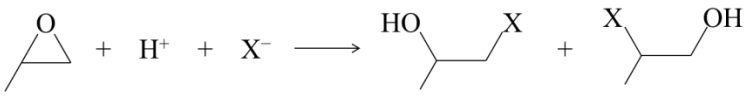

(3.1)

The increase of pH leads to hydrolysis and polycondensation of metal aquo complexes, and thus the metal (oxy)hydroxide/oxide gel can be obtained in an appropriate condition. Many metal oxide aerogels synthesized through epoxide-mediated method have been reported [28]. Combining the epoxide-mediated method and polymerization-induced spinodal decomposition, Al_2O_3, TiO_2, ZrO_2, and Fe_2O_3 HP monoliths have been prepared successfully [12, 17, 18, 20].

However, people found that it is still a challenge to prepare an oxide gel or HP monolith derived from low-valence metal salts, such as Mg, Mn (II), Co (II), Ni (II), Cu (II), Zn and so on [28], although some of them have been synthesized via epoxide-mediated method and reported [29–31]. We anticipated the difficulty can be due to the low electronegativity of central metal atoms (Table S1). The hydrolysis and polycondensation can be promoted even with atmospheric humidity by nucleophilic reactions [32]. According to the partial-charge model developed by Livage and his coworkers, the partial charge on metal atoms of most metal alkoxides is much higher than that on Si of silicon alkoxide [33]. As a result, the hydrolysis and polycondensation of metal alkoxides

become too fast to form a homogeneous gel with an extended network. Even in the epoxide-mediated method, it is difficult to form a homogeneous gel from solution of low-valence metal salts, since they generally have higher positive partial charge than high-valence metal cations. Employment of organic molecules or polymers as structure supporters to facilitate gelation is a common strategy [34–36]. However, the networks of these gels are constructed by the interaction between organic supporters and metal-based species rather than polycondensation of metal-based species. As a result, the monolithic form and original macroporous structure can hardly be preserved when the organic moieties are removed by heat treatment in air.

In the present report, we demonstrate a versatile preparation method of HP monoliths from three kinds of low-valence metal salts. The results and discussion will be divided into three parts, *i.e.* "gel formation", "phase separation", and "heat treatment". In the part of "gel formation", we will introduce the way to overcome the difficulty of homogeneous gelation for low-valence metal cation. Here, the starting materials are referred to the work reported by Hope-Weeks' group, but the process and mechanism in our work are different from theirs [31]. In the part of "phase separation", the effect of starting compositions on 3D interconnected macroporous structure of HP monoliths is discussed. Three factors to control the 3D interconnected macropores are introduced: the concentration of polymer (Cu-based system), the average molecular weight of polymer (Co-based system), and the amount of hydrochloric acid (Mn-based system). In the part of "heat treatment", the macroporous structure and crystalline phase of the heat-treated samples are presented.

3.2 Experimental

3.2.1 Starting materials

Copper (II) bromide ($CuBr_2$, > 99 %), cobalt (II) bromide ($CoBr_2$, > 99 %), manganese (II) bromide ($MnBr_2$, > 98 %), polyvinylpyrrolidone (PVP-40k, M_v = 40 000 Da), and poly(ethylene oxide)s (PEO-100k, PEO-200k, PEO-600k, M_v = 100 000, 200 000, 600 000 Da, respectively) were purchased from Sigma–Aldrich Japan. *N*,*N*-dimethylformamide (DMF, > 99.5 %), hydrochloric

acid (HCl, 35 ~ 37 %), distilled water (H_2O), 2-propanol (IPA, > 99 %), and *n*-hexane (> 95 %) were purchased from Kishida Chemical Co., Ltd. (Japan). Epichlorohydrin (ECH, > 99 %) was purchased from Tokyo Chemical Ind. Co., Ltd. (Japan). All the agents were used without further purification.

3.2.2 Preparation of HP monoliths

In a general preparation process, PVP and PEO were dissolved in DMF by heating under stirring. After the polymers dissolved and the solution cooled down to room temperature (r.t.), ECH was added. The mixed solution was transferred to the screw tube bottle, in which contained MBr_2 (M = Cu, Co, Mn). The solution was stirred in an ice-bath for 30 min after MBr_2 dissolved completely. Finally, HCl aqueous solution (35 ~ 37 %), diluted by H_2O in the volume ratio of 1:1, was added into the solution in the ice-water bath under stirring, followed by stirring for 5 s. The resulted solution was tightly sealed and placed in an ice-water bath for 1 h to allow the gelation. The M-based gel was subsequently aged at 25 °C (M = Cu, Co) or 60 °C (M = Mn) for 24 h. The gel was dried in a loosely capped bottle at 40 °C after solvent exchanges with IPA and *n*-hexane at 40 °C for least 8 h in each time, each for twice. The crystalline samples were heat-treated at varied temperatures for 2 h with the heating rate of 0.25 °C min^{-1} to target temperature in furnace. (For the specific amounts of materials, please see the Table 3.1)

Table 3.1 Starting compositions in respective systems.

	PEO-100k / mg	PVP-40k / mg	DMF / mL	ECH / mL	HCl aq. / mL
$CuBr_2$ 3 mmol	Varied	varied	1	1.5	0.1
$CoBr_2$ 4 mmol	Varied	50	1.5	2.5	0.15
$MnBr_2$ 4 mmol	40	60	1.5	2.5	varied

3.2.3 Characterization

The structures of the resultant samples in the micrometer range were examined using scanning electron microscopy (SEM, JSM-6060S, JEOL, Japan). The Fourier transform infrared (FT-IR) spectra were obtained using a FT-IR spectrometer with attenuated total reflection (ATR) method (IRTracer-100, Shimadzu Co., Japan). The macropore size distributions were determined using a mercury porosimeter (Autopore IV 9505, Shimadzu Co., Japan). Nitrogen adsorption–desorption isotherms obtained using a BELSORP-mini II (Microtrac BEL, Japan). The specific surface areas calculated from adsorption branch by Brunauer–Emmett–Teller (BET) method. The mesopore size distributions were calculated from the adsorption branch of the isotherm using Barrett–Joyner–Halenda (BJH) method. The crystalline structures of the samples were investigated using an X-ray diffractometer (XRD; SmartLab, Rigaku Co., Japan).

3.3 Results and discussion

3.3.1 Gel formation

The hydrolysis and polycondensation in acid condition are determined by the partial negative charge on oxygen. Here, the highly electronegative Br is expected to rearrange the distributions of electron density around metal and oxygen upon the formation of brominated metal alkoxide. In the present reaction, the brominated metal alkoxide is formed by an incomplete ring-opening reaction between epichlorohydrin (ECH) and metal bromides (MBr_2, M = Cu, Co, Mn), as expressed in Eq. 3.2.

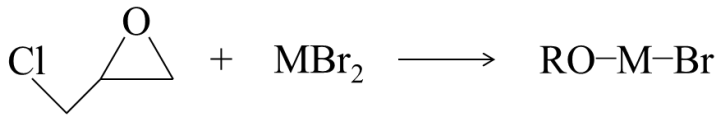

R = −CH(CH_2Br)CH_2Cl and −CH_2CHBrCH_2Cl (3.2)

The reaction between MBr_2 and ECH was carried out in the aprotic solvent, *N*,*N*-dimethylformamide (DMF), to allow the epoxide to react only with metal salt [37]. While DMF can dissolve metal salts, it cannot solvate the anions completely [38–40]. The choice of epoxide is based on two considerations: first, the reactivity toward metal salts; second, the resulted alkoxide group, which will have an effect on the hydrolysis rate. The kind of metal salts can be chosen based on following considerations: first, the electronegativity of anion; second, the difficulty of removal of the anion through post-treatment; third, the solubility in the solvent.

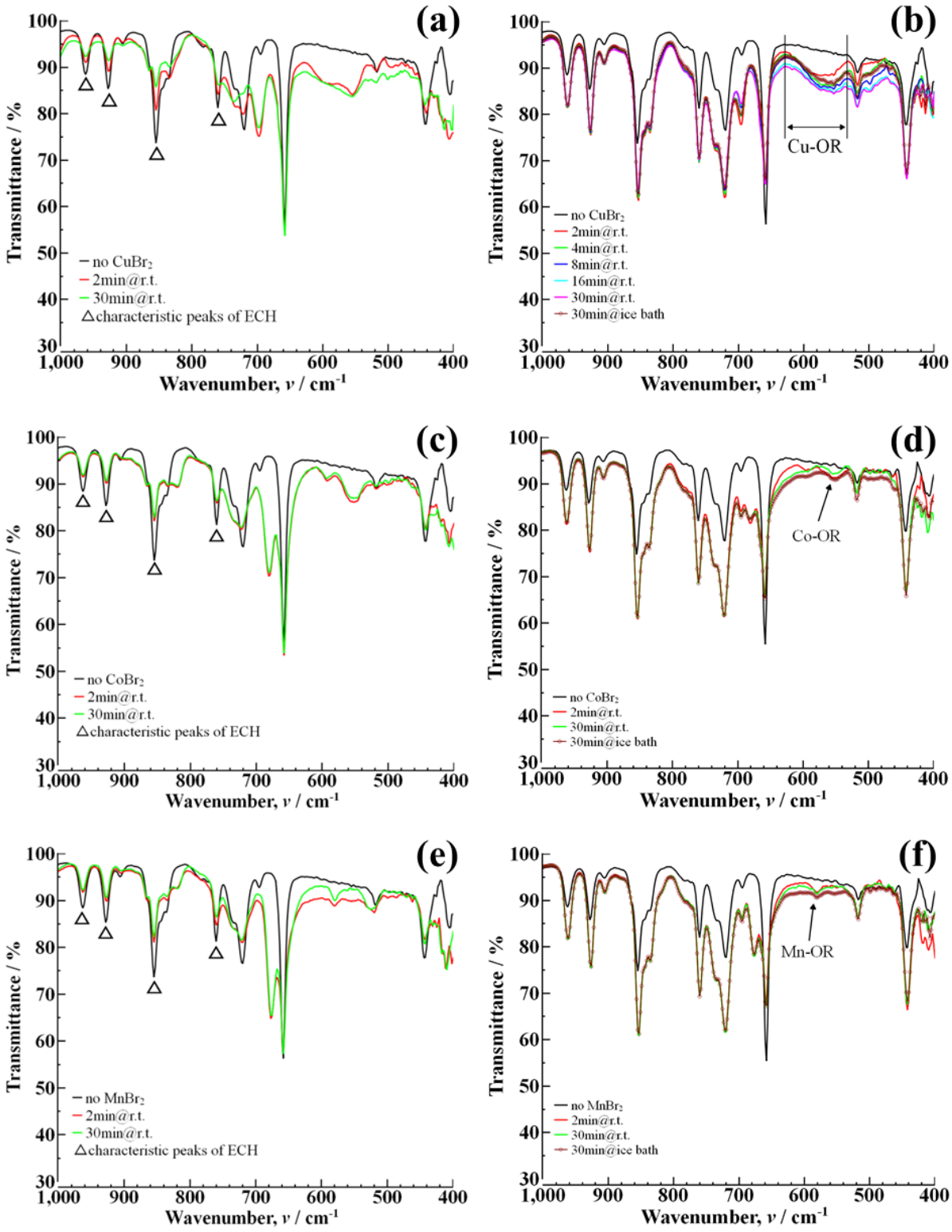

Figure 3.1 FT-IR spectra of control solution with the stoichiometric ratio of ECH to (a) $CuBr_2$, (c) $CoBr_2$, (e) $MnBr_2$ equal to 2:1 over time; solution with practical stoichiometric ratio of ECH to (b) $CuBr_2$, (d) $CoBr_2$, (f) $MnBr_2$ over time.

The reactions between ECH and MBr_2 were qualitatively confirmed by FT-IR spectroscopy. Considering the high mole ratios of ECH to MBr_2 (n_{ECH}/n_{Cu} = ~ 6.5, $n_{ECH}/n_{Co\ (or\ Mn)}$ = ~ 8.1) in the practical starting solutions, the control solutions containing ECH and MBr_2 with the mole ratio of 2:1 were characterized also by FT-IR to illustrate the reactions. In Cu-systems, the absorption of characteristic peaks of the epoxy ring (962, 928, 853, and 760 cm^{-1}) is decreased over time, but do not disappear completely within 30 min at r.t. (Figure 3.1(a)) [41]. On the other hand, the presence of the new absorption band ranged from 628 to 532 cm^{-1} is attributed to the formation of Cu–OR bonding [42–44]. Similar results were obtained in Co- and Mn-systems (Figure 3.1(c) and 3.1(e)).

Figure 3.1(b) shows the FT-IR spectra of the solutions with practical starting composition in Cu-based system. The new absorption band of Cu–OR vibration became stronger with the reaction time from 2 to 30 min at r.t. However, this absorbance in the solution, which was stirred in an ice-bath for 30 min after the $CuBr_2$ dissolved completely, is close to that of the sample with the reaction time within 4 min at r.t. It means the ring-opening reaction can be slowed down (or stopped) effectively by cooling in an ice-bath. According to all the results above, it can be concluded that the ECH will react with $CuBr_2$ via ring-opening reaction to form alkoxide groups, and this reaction can be slowed down (or stopped) in an ice-cooled condition. It can be reasonably deduced that brominated copper alkoxides ($CuBr_x(OR)_y$) with Br ligands and OR groups were produced in the starting solution composition due to the incomplete reaction between ECH and $CuBr_2$. In addition, it implies that the relative numbers of Br ligand and OR group can be adjusted by controlling the reaction process via reaction time and temperature, and thus the reactivity of brominated metal alkoxides can be controlled. The use of brominated precursor allows one to prepare a homogeneous composite oxides gel, where moderate rates of hydrolysis and polycondensation of the precursors are essential.

There are some differences of absorption peaks attributed to M–OR vibration with varied conditions and reaction times in Co- and Mn-systems (Figure 3.1(d) and 3.1(f)). From the Figure 3.1(c) and 3.1(e), the absorptions of characteristic peaks of the epoxy ring have negligible change with the reaction time from 2 to 30 min at r.t. It indicates that the reaction equilibrium between $M'Br_2$ (M' = Co, Mn) and ECH are nearly reached within 2 min at r.t. Nevertheless, it also can be

deduced that the brominated alkoxides with Br ligands and OR groups are produced in Co- and Mn-systems.

After the formation of Br–M–OR intermediates, subsequent processes may be essentially similar to the hydrolysis and polycondensation of silicon alkoxides, which have been well investigated. Due to the presence of highly electronegative Br ligand, the electron density on the oxygen atom in alkoxy ligand relatively decreases. At the same time, bulky halogenated propyl ligand causes steric hindrance toward hydrolysis, thus slows down the hydrolysis rate. On the other hand, the polycondensation between M−OH is also slowed down due to the presence of Br ligand. As a result, a monolithic gel consisting of with M–O–M network can be prepared by this method.

3.3.2 Phase separation

$$\Delta G \propto RT\left(\frac{\Phi_g}{P_g}\ln\Phi_g + \frac{\Phi_s}{P_s}\ln\Phi_s + \chi_{gs}\Phi_g\Phi_s\right) \quad (3.3)$$

The phase separation tendency can be estimated qualitatively by Flory–Huggins equation (Eq. 3.3), where ΔG is Gibbs free energy change of mixing; R is the gas constant; T is the temperature; Φ is the volume fraction; P is the degree of polymerization; g and s express gel-rich phase and solvent-rich phase, respectively; χ_{gs} is the interaction parameter between components in gel-rich and solvent-rich phases, which describes the compatibility between two components [45, 46]. The former two terms in the bracket express the entropic contribution, and the last term expresses the enthalpic contribution. Since the value of Φ ranged from 0 to 1, the entropic term is negative. The enthalpic term can be negative or positive, which depends on χ_{gs}. Under a condition where χ_{gs} is positive, the degree of polymerization in gel-rich phase, P_g will be increased with the proceeding of polycondensation. The entropic term thus becomes less negative. When the absolute value of entropic term becomes small enough until ΔG becomes positive, the system becomes unstable, and phase separation occurs. In addition, other parameters, such as the degree of polymerization in solvent-rich phase, P_s, volume fraction, Φ, and interaction parameter, χ_{gs} also have effects on the phase separation tendency. Here, we will present how to control the phase-separated morphology

by different experimental parameter based on the Flory–Huggins equation in the next three systems, respectively.

3.3.2.1 *Cu-system*

In most cases of our previous works, PEO was employed to induce the phase separation, and the PEO was preferentially distributed to the solvent-rich phase [5, 10, 12, 23]. As shown in the SEM images, the morphologies of Cu-based as-dried gels changed from nanoporous to 3D interconnected macroporous when the amount of PEO-100k increased from 35 to 60 mg (Figure 3.2(a)–(d)). This change can be interpreted as follows; with an increase of starting PEO-100k concentration, the volume fraction of PEO–solvent rich phase increases accompanied by the increase of phase separation tendency. However, the concentration of PEO-100k has limited effects on the domain size of gel-rich phase, as the size of skeleton showed negligible changes. Besides, the domain size of PEO–solvent phase cannot be further increased by adding more PEO-100k due to the poor solubility of PEO-100k in the DMF. For the purpose of controlling the sizes of macropore and skeleton over a wider range, additional polymer, PVP-40k, was employed [5, 23]. As the amount of PVP-40k was increased from 0 to 50 mg with a fixed amount (35 mg) of PEO-100k, the morphology changed from nanoporous to 3D interconnected macroporous (Figure 3.2(e)–(g)). When the amount of PVP-40k increased to 50 mg, particle-like structure could be found due to the secondary phase separation. The phase-separated morphology was observed when the amount of PVP-40k was increased to 5 mg with a fixed amount of PEO-100k. The skeleton becomes coarser with an increase of PVP-40k. PVP is considered to be mainly distributed to the gel-rich phase due to the attractive interaction between carbonyl groups to Cu-based oligomers. The interaction between PVP and Cu-based oligomers make the composite in gel-rich phase less compatible against that in solvent-rich phase, leading to the higher phase separation tendency. In this way, the addition of PVP-40k resulted in not only increasing the size of skeleton, but also increasing size of macropore. The morphologies of other samples prepared with varied amounts of PEO-100k and PVP-40k are summarized in Figure 3.2(h). According to the current results, the compositional ranges favorable for phase separated (interconnected) macroporous morphology have been

confirmed. For example, the phase separation can hardly be induced when the amount of PEO-100k less than 30 mg; with the increase of PEO-100k, the variable range of PVP-40k (for interconnected morphology) becomes narrow. It thus becomes possible to prepare the desired sizes of macropores and skeletons by varied concentrations of PEO-100k and PVP-40k. The macropore sizes of the samples prepared with 10, 20, 30, and 40 mg of PVP are 0.23, 0.43, 0.55, 1.02 μm, respectively, and have sharp distributions (Figure 3.2(i)). Meanwhile, the mesopore sizes of all four samples are around 5 nm, which is affected negligibly by the amount of PVP-40k, but mostly determined by sol–gel transition and drying process. Therefore, the sizes of macropore and mesopore can be controlled independently. The specific surface areas of the samples prepared with 10, 20, 30, and 40 mg of PVP, calculated by Brunauer–Emmett–Teller (BET) method are 61, 58, 38, 30 $m^2 g^{-1}$, respectively. The mesopore size shows a negligible change, but the pore volume decreases with the increase of PVP. Therefore, the specific surface area decreased with increasing the amount of PVP.

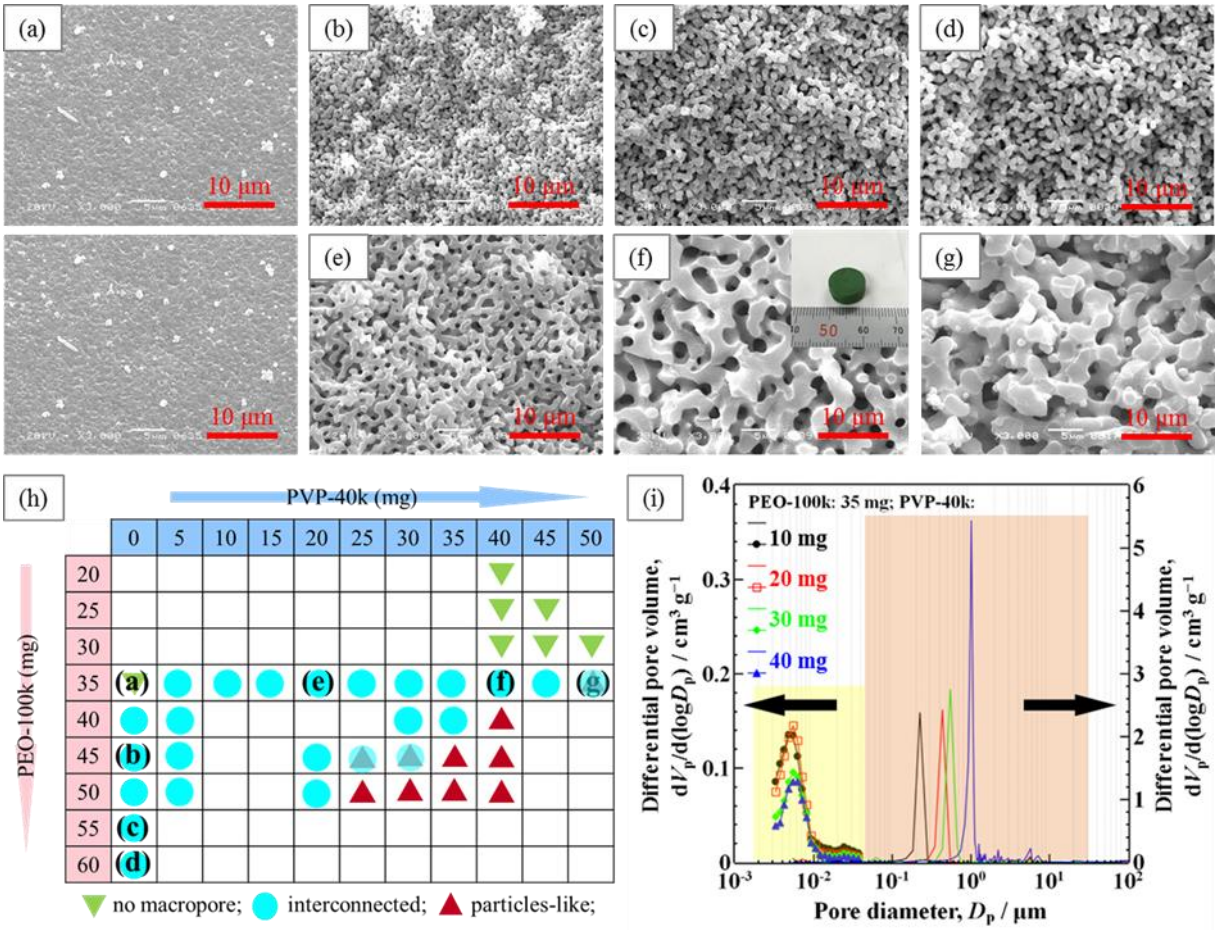

Figure 3.2 (a)–(g) SEM images of Cu-based as-dried samples prepared with varied concentrations of PVP-40k and PEO-100k; the inserted photo in (f) is the appearance of the Cu-based as-dried sample. (h) Dependence of resultant samples morphology on starting polymer composition. (i) Pore size distributions of Cu-based as-dried samples prepared with varied concentration of PVP-40k: The macropore size distribution was obtained by mercury intrusion porosimetry, and the mesopore size distribution was obtained by nitrogen adsorption–desorption measurement.

3.3.2.2 *Co-system*

In contrast to the Cu-system, the phase separation tendency in the Co-system is relatively weak at any possible concentrations of PEO-100k and PVP-40k. In other words, the domain sizes of gel-rich phase and solvent-rich phase can hardly be controlled in this condition (Figure 3.3(a)–(c)). In the Co-system, PEO is also considered to be preferentially distributed to solvent-rich phase. The phase separation is driven by the entropy loss due to the polymerization of cobalt-species and

thus depends directly on the molecular weight of respective constituents [16]. The phase separation took place with smaller amount of PEO-200k compared with the case of PEO-100k, as shown in the Figure 3.3(d). On the other hand, gels prepared with PEO-200k had coarser skeletons and larger macropores compared with the gels prepared with PEO-100k (Figure 3.3(e)). However, the phase separation was not further enhanced by the use of 50 mg of PEO-200k (Figure 3.3(f)). Substantially high viscosity of the reaction solution is considered to have suppressed the coarsening of phase-separated structure before gelation [47]. The gels with coarser skeletons and larger macropores can be obtained using PEO with higher average molecular weight, *e.g.* PEO-600k (Figure 3.3(g)–(i)). It was found that smaller amounts of PEO were required to obtain phase-separated structures when the PEO with higher molecular weight was employed. Besides, the morphology of the samples was sensitive to the amount of PEO-600k. As shown in the SEM images, both sizes of macropore and skeleton were increased as the amount of PEO-600k changed from 20, to 25, and 30 mg. These results indicate that PEO with higher molecular weight gives a higher phase separation tendency and thus can induce phase separation at a lower concentration. Therefore, the 3D interconnected macropores in the Co-system can be controlled by concentration and average molecular weights of PEO. Furthermore, it will be similarly applicable to other systems where PEO and metal-based oligomers have weak attractive interactions between each other. The nitrogen adsorption isotherms show an uptake at low relative pressure indicative of high specific surface area (Figure 3.3(j)). The specific surface areas calculated by BET method are 244 (PEO-100k: 80 mg), 284 (PEO-200k: 45 mg), and 112 (PEO-600k: 25 mg) $m^2\ g^{-1}$, respectively. The considerable uptake in the intermediate relative pressure range together with adsorption–desorption hysteresis implies the presence of mesopores. Similar mesopore size distributions, which derived from Barrett–Joyner–Halenda (BJH) method, are observed in the samples prepared by PEO-100k and PEO-200k, while the pore size distribution shifts to the larger region in the sample prepared by PEO-600k (Figure 3.3(k)). That is the reason why the specific surface area of the sample prepared by PEO-600k is much lower than those of the samples prepared by PEO-100k and PEO-200k.

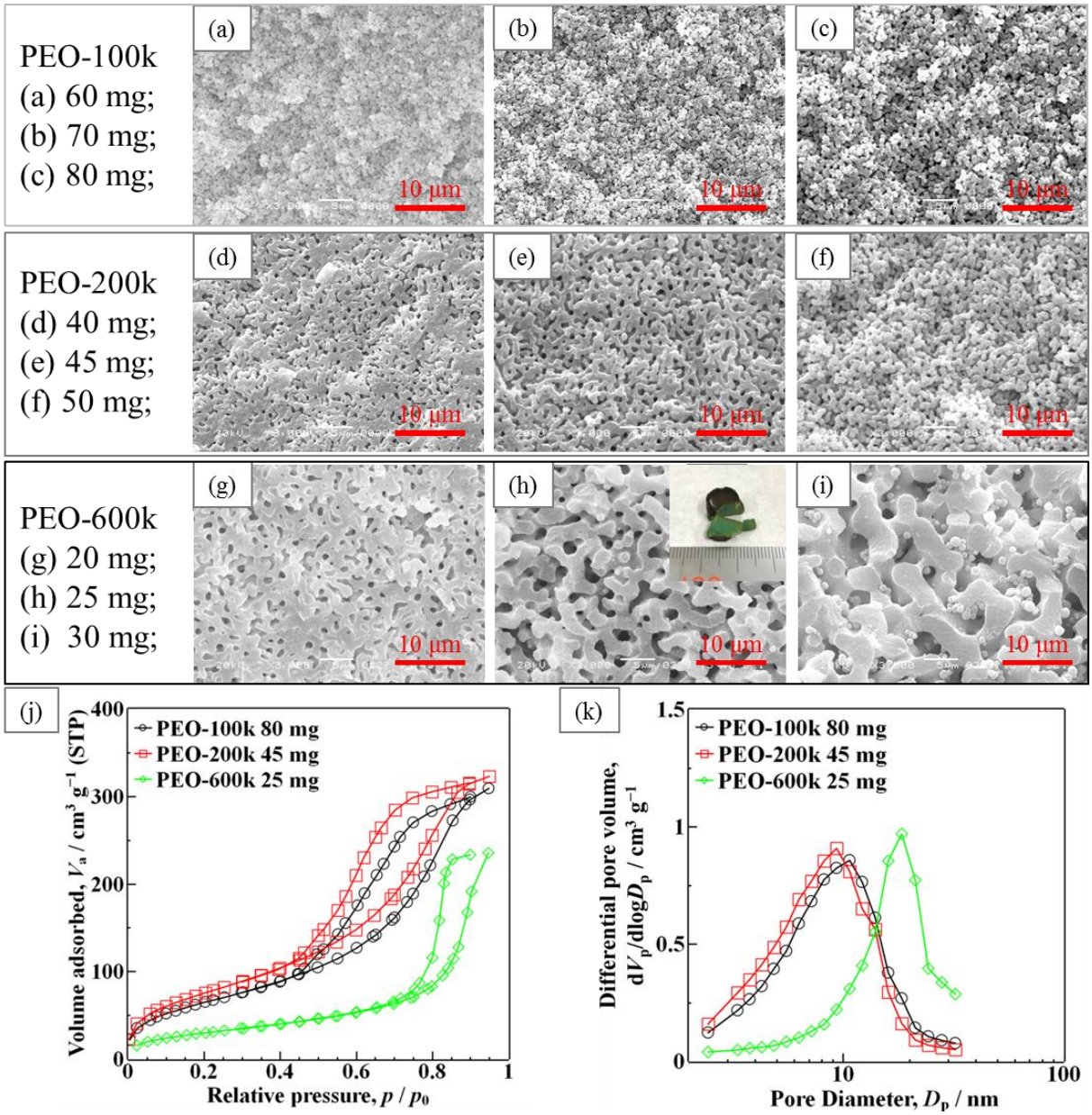

Figure 3.3 SEM images of Co-based as-dried samples prepared with varied amounts and average molecule weights of PEO. PEO-100k: (a) 60 mg; (b) 70 mg; (c) 80 mg; PEO-200k: (d) 40 mg; (e) 45 mg; (f) 50 mg; PEO-600k: (g) 20 mg; (h) 25 mg; (i) 30 mg. PVP-40k: 50 mg for all samples. The inserted photo in (h) is the appearance of the Co-based as-dried sample. The brown color in the surface is because the sample was oxidized into CoO(OH) in air. (j) Nitrogen adsorption isotherms and (k) mesopore size distributions of the Co-based as-dried samples prepared with different PEO.

3.3.2.3 *Mn-system*

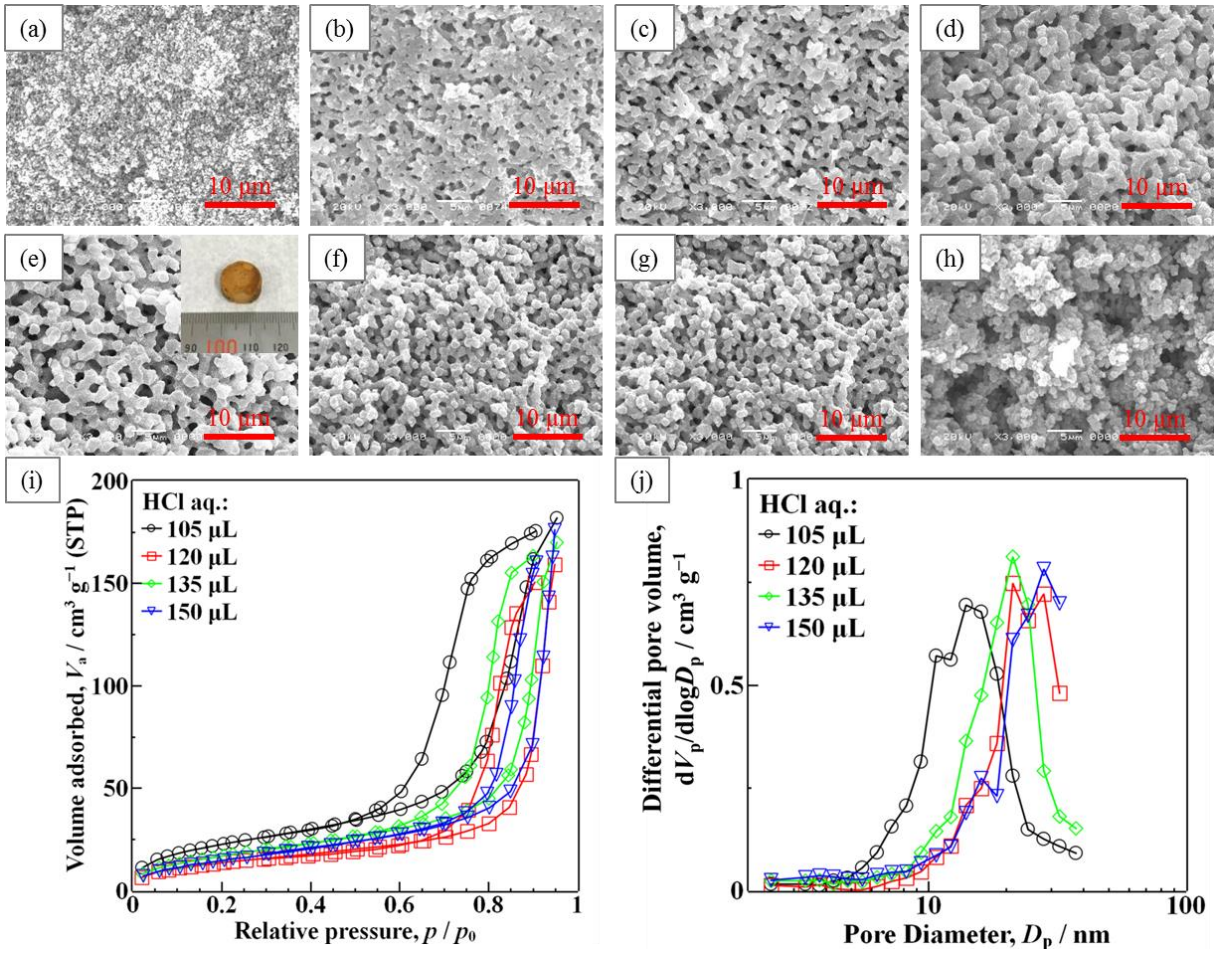

Figure 3.4 SEM images of Mn-based as-dried samples prepared with varied amounts of HCl aq: (a) 75 μL; (b) 90 μL; (a) 105 μL; (c) 120 μL; (d) 135 μL; (e) 150 μL; (f) 165 μL; (h) 180 μL; the inserted photo in (e) is the appearance of the Mn-based as-dried sample. (i) Nitrogen adsorption isotherms and (j) mesopore size distributions of the Mn-based as-dried samples prepared with varied amounts of HCl aq. PEO-100k: 40 mg, PVP-40k: 60 mg for all samples.

The morphology with pores in micrometer scale is a result of the competitive processes of sol–gel transition and phase separation. Any factor affecting sol–gel transition, such as temperature, catalyst, concentration, and those affecting phase separation, such as polymerization, compatibility between constituents, will determine the final morphology of the sample, which has been well investigated by Nakanishi [16]. It indicates that the 3D interconnected macropore can be

controlled not only by additive polymer, but also by other parameters. Figure 3.4 shows the SEM images of Mn-based as-dried gels prepared with varied amounts of diluted HCl aqueous solution (HCl aq.) from 75 to 180 μL. No 3D interconnected macropore was observed in the sample prepared by 75 μL HCl aq. (Figure 3.4(a)). The 3D interconnected macropore became larger when the amount of HCl aq. increased from 90 to 135 μL (Figure 3.4(b)–(e)). It is a result of two combined effects: first, the higher water concentration increases the polarity of solvent-rich phase, which lowers the compatibility of hydrophobic Mn-based-oligomer–PVP, and thus enhances the phase separation tendency; second, the volume fraction of solvent-rich phase was increased. However, the skeletons and macropores became finer when the amount of HCl aq. was further increased from 135 to 165 μL (Figure 3.4(e)–(g)). This is because the more HCl aq. accelerated the hydrolysis and polycondensation of Mn−OR and hence made the gelation occur in the earlier stage of phase separation and prevent the phase-separated structure from coarsening. When the added amount of HCl aq. reached 180 μL, the sol–gel transition became much faster and the volume fraction of solvent-rich phase became higher. As a result, macroporous but disordered structure was obtained (Figure 3.4(h)). The amount of HCl aq. also affected the pH of the solvent in which wet gels were aged. The nitrogen adsorption isotherms and the corresponding BJH mesopore size distributions shown in Figure 3.4(i)–(j) confirm that the resultant mesopores become larger roughly corresponding to the amount of HCl aq. The specific surface areas of the samples prepared with 105, 120, 135, and 150 μL of HCl aq., calculated by BET method are 84, 50, 65, 57 m^2 g^{-1}, respectively. The results indicate the possibility of using varied amounts of HCl aq. to control the mesopore size.

3.3.3 Heat treatment

All the as-dried samples in three systems are amorphous under XRD (may contain fine crystallites). Heat treatment under oxidative conditions is necessary for obtaining fully crystalline phases and removing the organic moieties in the skeleton. All the crystalline oxides can be obtained after careful heat treatment in air with their 3D interconnected macroporous structures preserved, although isotropic shrinkages occurred (Figure 3.5). In Cu-system, although the 3D

interconnected macropores can be preserved, the monolith cracks into pieces after heat-treatment (Figure 3.5(a) and 3.5(b)). Crystalline CuO was obtained after heat-treated in air at 300 °C for 2 h, but some impurity phases were found according to the XRD pattern (Figure 3.5(c)). Heat treatment at higher temperature (*e.g.* 400 °C) can remove the impurity, but at the same time the original morphology is destroyed resulting in very fragile heat-treated sample. This may be because other crystals, such as CuBr, Cu, Cu_2O, will form in the process of heating up. The volume changes caused by the repeated changing of crystalline structures might lead to the deformation and collapse. In Co-system, not only the macroporous structure, but also the monolithic form can be preserved after heat-treated in air at 300 °C (Figure 3.5(d) and 3.5(e)). Crystalline Co_3O_4 without any impurity was obtained (Figure 3.5(f)). The macroporous structure and monolithic form can be preserved even after heat-treatment at higher temperatures, resulted in higher crystallinity of Co_3O_4. In Mn-system, crystalline Mn_5O_8 without losing the original 3D interconnected macropores was obtained after heat treatment, although an isotropic shrinkage and crack formation took place (Figure 3.5(g)–(i)). In addition, other crystalline phases, such as Mn_2O_3, Mn_3O_4 can also be obtained by heat-treatment with varied target temperatures and heating rates.

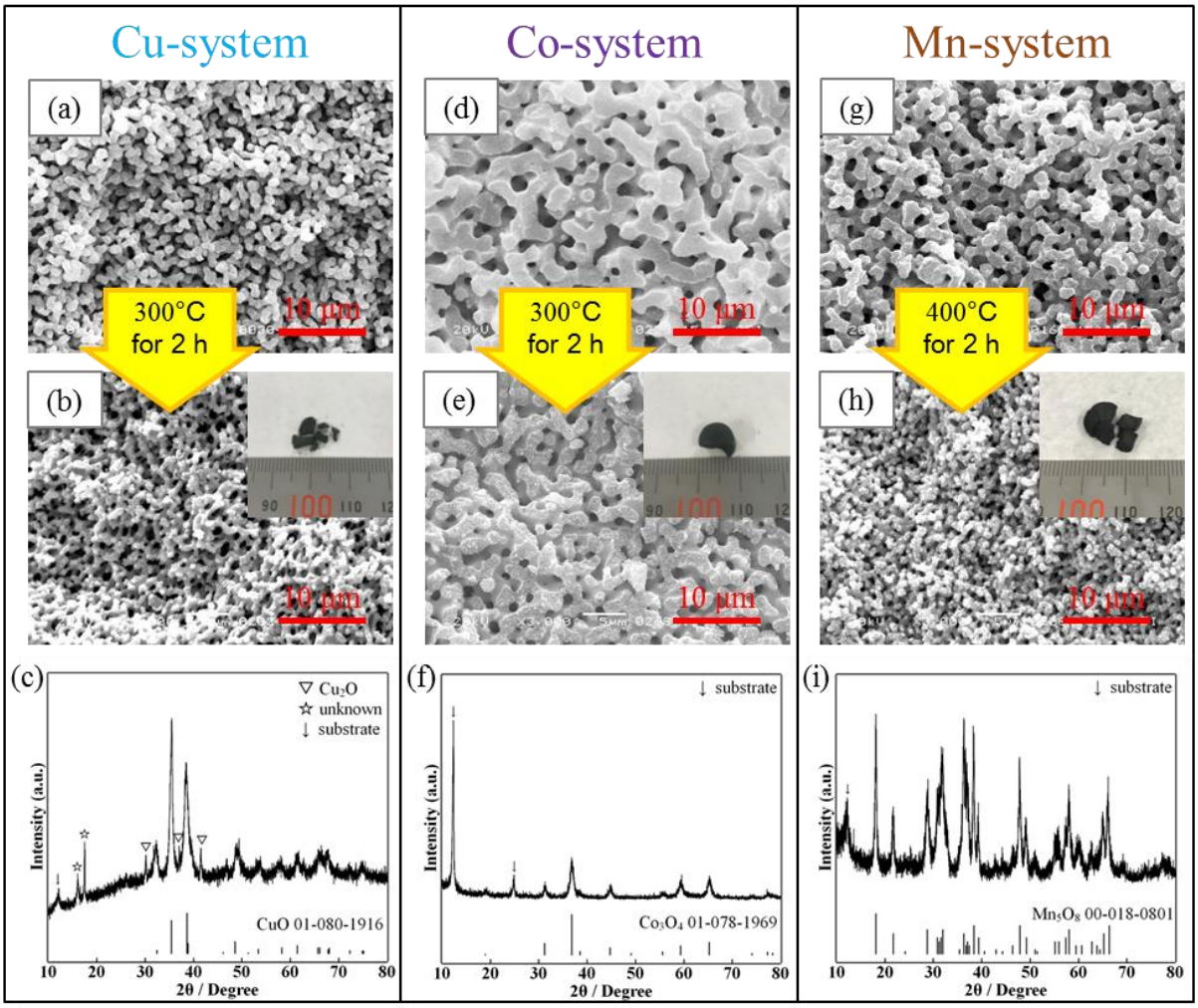

Figure 3.5 SEM images of the as-dried and heat-treated samples (inserted photos are the appearance of heat-treated samples), and XRD patterns of heat-treated samples in Cu-system (a)–(c); in Co-system (d)–(f); in Mn-system (g)–(i), respectively.

3.4 Conclusions

Monolithic gels based on low-valence transition metal (Cu, Co, Mn) oxides have been prepared successfully through hydrolysis and polycondensation of the brominated metal alkoxides, which are the products of the reaction between MBr_2 and ECH. The remaining Br decreases the partial positive/negative charge on metal/oxygen, and thus decreases the rates of hydrolysis and

polycondensation. The open mesopores with sharp distribution in the monoliths are the natural result of sol–gel process. The 3D interconnected macropores are obtained by addition of two kinds of organic polymers, PEO and PVP to induce the phase separation. The domain sizes of skeleton and macropore can be controlled by the concentration and the average molecular weight of polymers, and the amount of HCl aq. After heat treatment in air, the crystalline metal oxides without destroying their 3D interconnected macroporous structures (in all the systems) and monolithic form (in Co- and Mn-system) can be obtained. This study illuminates the difficulty of the gelation for low-valence (or lowly electronegative) metal cations, and provides a novel route to prepare low-valence metal based gels and HP monoliths. The systemic controlling mesoporous size through surfactants, sol–gel transition, drying, and heat treatment to meet the practical applications will be our future work.

References

[1] K. Nakanishi, N. Tanaka, *Acc. Chem. Res.* **2007**, *40*, 863.

[2] O. Núñez, K. Nakanishi, B. Tanaka, *J. Chromatogr. A* **2008**, *1191*, 231.

[3] G. Hasegawa, K. Morisato, K. Kanamori, K. Nakanishi, *J. Sep. Sci.* **2011**, *34*, 3004.

[4] R. Ito, K. Morisato, K. Kanamori, K, Nakanishi, *J. Sol–gel Sci. Technol.* **2019**, *90*, 105.

[5] G. Hasegawa, Y. Ishihara, K. Kanamori, K. Miyazaki, Y. Yamada, K. Nakanishi, T. Abe, *Chem. Mater.* **2011**, *23*, 5208.

[6] G. Hasegawa, A. Kitada, S. Kawasaki, K. Kanamori, K. Nakanishi, Y. Kobayashi, H. Kageyama, T. Abe, *J. Electrochem. Soc.* **2015**, *162*, A77.

[7] G. Hasegawa, K. Kanamori, N. Kannari, J. Ozaki, K, Nakanishi, T. Abe, *J. Power Sources* **2016**, *318*, 41.

[8] G. Hasegawa, K. Kanamori, T. Kiyomura, H. Kurata, T. Abe, K. Nakanishi, *Chem. Mater.* **2016**, *28*, 3944.

[9] H. Li, D. Yuan, C. Tang, S. Wang, J. Sun, Z. Li, T. Tang, F. Wang, H. Gong, C. He, *Carbon* **2016**, *100*, 151.

[10] Y. Zhu, T. Shimizu, T. Kitajima, K. Morisato, N. Moitra, B. Nicolas, T. Kiyomura, K. Kanamori, K. Takeda, H. Kurata, M. Tafu, K. Nakanishi, *New J. Chem.* **2015**, *39*, 2444.

[11] W. Yuan, P. Yuan, D. Liu, W. Yu, L. Deng, F. Chen, *Micropor. Mesopor. Mat.* **2015**, *206*, 184.

[12] Y. Hara, K. Kanamori, K. Morisato, R. Miyamoto, K. Nakanishi, *J. Mater. Chem. A* **2018**, *6*, 9041.

[13] D. Gao, Y. Shen, B. Zhao, Q. Liu, K. Nakanishi, J. Chen, K. Kanamori, H. Wu, Z. He, M. Zeng, H. Liu, *ACS Sustainable Chem. Eng.* **2019**, *7*, 8512.

[14] F. Sayler, A. Grano, J. Smått, M. Lindén, M.G. Bakker, *Micropor. Mesopor. Mat.* **2014**, *184*, 141.

[15] C. Pélisson, T. Nakanishi, Y. Zhu, K. Morisato, T. Kamei, A. Maeno, H. Kaji, S. Muroyama, M. Tafu, K. Kanamori, T. Shimada, K. Nakanishi, *ACS Appl. Mater. Interfaces* **2017**, *9*, 406.

[16] K. Nakanishi, *J. Porous Mater.* **1997**, *4*, 67.

[17] W. Li, X. Guo, Y. Zhu, Y. Hui, K. Kanamori, K. Nakanishi, *J. Sol–gel Sci. Technol.* **2013**, *67*, 639.

[18] Y. Tokudome, K. Fujita, K. Nakanishi, K. Miura, K. Hirao, *Chem. Mater.* **2007**, *19*, 3393.

[19] J. Konishi, K. Fujita, S. Oiwa, K. Nakanishi, K. Hirao, *Chem. Mater.* **2008**, *20*, 2165.

[20] X. Guo, J. Song, Y. Lvlin, K. Nakanishi, K. Kanamori, H. Yang, *Sci. Technol. Adv. Mater.* **2015**, *16*, 025003.

[21] Chapter 2 in the present thesis.

[22] Y. Tokudome, A. Miyasaka, K. Nakanishi, T. Hanada, *J. Sol–gel Sci. Technol.* **2011**, *57*, 269.

[23] Y. Zhu, K. Yoneda, K. Kanamori, K. Takeda, T. Kiyomura, H. Kurata, K. Nakanishi, *New J. Chem.* **2016**, *40*, 4153.

[24] K. Nakanishi, N. Soga, *J. Am. Ceram. Soc.* **1991**, *74*, 2518.

[25] J. Konishi, K. Fujita, K. Nakanishi, K. Hirao, *Chem. Mater.* **2006**, *18*, 6069.

[26] G. Hasegawa, K. Kanamori, K. Nakanishi, T. Hanada, *J. Am. Ceram. Soc.* **2010**, *93*, 3110.

[27] T. F. Baumann, A. E. Gash, J. H. Satcher Jr., A robust approach to inorganic aerogels: the use of epoxides in sol–gel synthesis. In: *Aerogel Handbook*. Aegerter M (ed.) Switzerland: Springer, **2011**, 155.

[28] A. E. Gash, T. M. Tillotson, J. H. Satcher Jr., L. W. Hrubesh, R. L. Simpson. *J. Non-Cryst. Solids* **2001**, *285*, 22.

[29] A. E. Gash, J. H. Satcher Jr., R. L. Simpon, *J. Non-Cryst. Solids* **2004**, *350*, 145.

[30] T. Wei, C. Chen, K. Chang, S. Lu, C. Hu, *Chem. Mater.* **2009**, *21*, 3228.

[31] R. Baghi, G. R. Peterson, L. J. Hope-Weeks, *J. Mater. Chem. A* **2013,** *1*, 10898.

[32] C. J. Brinker, G. W. Scherer. Hydrolysis and condensation I: nonsilicates. In: *Sol–gel Science*. United States: Academic Press, **1990**, 21–95.

[33] J. Livage, M. Henry, C. Sanchez, *Prog. Solid St. Chem.* **1988**, *18*, 259.

[34] Y. Kido, K. Nakanishi, N. Okumura, K. Kanamori, *Micropor. Mesopor. Mat.* **2013**, *176*, 64.

[35] Y. Kido, G. Hasegawa, K. Kanamori, K. Nakanishi, *J. Mater. Chem. A* **2014,** *2*, 745.

[36] S. Fukumoto, K. Nakanishi, K. Kanamori, *New J. Chem.* **2015**, *39*, 6771.

[37] S. Dolci, F. Marchetti, G. Pampaloni, S. Zachini, *Dalton. Trans.* **2010**, *39*, 5367.

[38] W. Grzybkowski, M. Pilarczyk, *J. Chem. Soc. Faraday Trans. 1* **1986**, *82*, 1745.

[39] M. Pilarczyk, L. Klinszporn, *Electrochim Acta* **1986**, *31*, 185.

[40] M. Pilarczyk, W. Grzybkowski, L. Klinszporn, *Polyhedron* **1987**, *6*, 1399.

[41] F. Wang, P. Polavarapu, *J. Phys. Chem. A* **2000**, *104*, 6189.

[42] J. Singh, B. Baranwal, R. Mehrotra, *Z. Anorg. Allg. Chem.* **1981**, *477*, 235.

[43] F. Meyer, R. Hempelmann, S. Mathur, M. Veith, *J. Mater. Chem.* **1999**, *9*, 1755.

[44] R. L. Halbach, D. Gygi, E. D. Bloch, B. L. Anderson, D. G. Nocera, *Chem. Sci.* **2018**, *9*, 4524.

[45] P. Flory, *J. Chem. Phys.* **1942**, *10*, 51.

[46] M. Huggins, *J. Am. Chem. Soc.* **1942**, *64*, 2716.

[47] K. Nakanishi, N. Soga, *J. Non-Cryst. Solids* **1992**, *139*, 14.

Summary

The present thesis deals with the preparation of low-valence metal oxide hierarchically porous (HP) monolith and the control of the 3D interconnected macropores via sol–gel process accompanied by phase separation. The contents can be summarized in two topics as follows.

The first topic is “gel formation”. Preparation of a homogeneous gel is the core in preparing monolithic porous materials shown throughout the present thesis. Since the 3D interconnected macroporous structure is obtained through spatial arresting of the transient state in the process of phase separation by gelation, the gelation is one of the critical processes in this method. There are two necessary conditions for a system to form a gel: 1. the monomer and oligomer in the system possess enough reactive groups for polymerization in free (three-dimensional) space; 2. the oligomers should be dispersed homogeneously in the system before the gel formation. Theoretically, most of metal species satisfy the first requirement, because they can form 4- or 6-coordination complexes in the solution, and all of the ligand can be hydrolyzed. The essential problem is that many low-valence metal complexes have rapid rates of hydrolysis and polycondensation. The high reactivity can be attributed to the low electronegativity according to the partial charge model. As a result, only the precipitation is obtained rather than homogeneous gel. In order to prepare a gel from low-valence metal species, suppression of the precipitation and slowing down the hydrolysis and polycondensation are two alternative strategies.

In Mg-system, the monolithic gel can be obtained in solution with a low water/methanol ratio, without using any structure supporter. Polyvinylpyrrolidone (PVP), was only used to suppress the phase separation, although it was found in the gel-rich phase according to the TG-DTA and FT-IR results. Due to its moderate interaction with Mg-based oligomers, however, the majority of PVP is not molecularly included in the network upon gel formation. Therefore, the monolithic form and 3D interconnected macropores are not destroyed after removing the PVP by heat-treatment, although the mechanical strength is decreased. In Zn-system, the small molecule, citric acid, which has a strong interaction with Zn-based species, was used to facilitate the gelation. The

difference between the HP monolith prepared with small molecule and that prepared with organic polymer is, that the former product can contain a higher fraction of inorganic component. As a result, the 3D interconnected macropores can be preserved after heat-treatment. In Mn-, Co-, Cu-system, the monolithic gels were prepared via careful control of the rates of hydrolysis and polycondensation by introducing a highly electronegative atom, but not via use of the organic additive to suppress the precipitation. The M–O–M networks were formed in the wet gels. Therefore, the mechanical strength of the heat-treated samples was improved. The last method is considered to be effective to prepare HP monolith based on low-valence metal oxides.

The second topic is "phase separation". In Mg-system, since the magnesium hydroxide has a very low solubility in aqueous solutions, the PVP here acts as a phase separation inhibitor to control the final macroporous structure. In Zn-system, the phase separation is controlled by the respective volume fractions of the good solvent (methanol) and poor solvent (epoxide), without additional organic polymer. In Mn-, Co-, Cu-systems, two polymers: PVP and PEO are employed in combination. In Mn-system, the effect of diluted HCl aq. on the macroporous structure is presented. The amount of HCl aq. determines the polarity of solvent-rich phase, the volume fraction of solvent-rich phase, and the rates of hydrolysis and polycondensation. All the factors finally determine the morphology of the sample. In Co-system, the phase separation tendency can be increased using PEO with higher molecular weight. Thus the sizes of macropore and skeleton can be controlled by PEO with different molecular weights. In Cu-system, the sizes of macropore and skeleton are controlled by the amounts of PVP and PEO in a concerted way.

The present thesis demonstrates various methods to obtain monolithic gels from low-valence metal inorganic salt and to control the 3D interconnected macropores in the HP monoliths via phase separation.

List of Publications

Chapter 1

"Synthesis of Hierarchically Porous MgO Monoliths with Continuous Structure via Sol–gel Process accompanied by Phase Separation"

Xuanming Lu, Kazuyoshi Kanamori, Kazuki Nakanishi, *Journal of Sol–gel Science and Technology* **2019**, *89*, 29–36.

Chapter 2

"Preparation of Zinc Oxide with a Three-Dimensionally Interconnected Macroporous Structure *via* a Sol–Gel Method accompanied by Phase Separation"

Xuanming Lu, Kazuyoshi Kanamori, Kazuki Nakanishi, *New Journal of Chemistry* **2019**, *43*, 11720–11726.

Chapter 3

"Hierarchically Porous Monoliths based on Low-Valence Transition Metal (Cu, Co, Mn) Oxides: Gelation and Phase Separation"

Xuanming Lu, Kazuyoshi Kanamori, Kazuki Nakanishi

Under review

Other publications (not included in this thesis)

"A Novel Method to Modify the Color of VO_2-based Thermochromic Smart Films by Solution-Processed VO_2@SiO_2@Au Core-Shell Nanoparticles"

Xuanming Lu, Xiudi Xiao, Ziyi Cao, Yongjun Zhan, Haoliang Cheng, Gang Xu, *RSC Advance* **2016**,

6, 47249–47257.

"A Cost-Effective Method to Fabricate VO_2 (M) Nanoparticles and Films with Excellent Thermochromic Properties"
Hua Zhang, Xiudi Xiao, Xuanming Lu, Guanqi Chai, Yaoming Sun, Yongjun Zhan, Gang Xu, *Journal of Alloys and Compounds* **2015**, *636*, 106–112.

"A Simple and Low-Cost Combustion Method to Prepare Monoclinic VO_2 with Superior Thermochromic Properties"
Ziyi Cao, Xiudi Xiao, Xuanming Lu, Yongjun Zhan, Haoliang Cheng, Gang Xu, *Scientific Reports* **2016**, *6*, 39154–39162.

"Superelastic Multifunctional Aminosilane-Crosslinked Graphene Aerogels for High Thermal Insulation, Three-Component Separation, and Strain/Pressure-Sensing Arrays"
Guoqing Zu, Kazuyoshi Kanamori, Kazuki Nakanishi, Xuanming Lu, Kunhua Yu, Huang Jia, Hiroyushi Sugimura, *ACS Applied Materials & Interfaces* **2019**, *11*, 43533–43542.

Acknowledgement

I would like to sincerely thank the following people who supported me during my whole PhD education.

Much thank to my supervisor, Professor Dr. Hiroshi Kitagawa, for his support on my doctoral course.

Much thank to my supervisor, Professor Dr. Kazuki Nakanishi, for his professional and patient guidance. Thanks for every inspiring discussion on my research and careful revision of my writing. Thanks to his effort, I can present this thesis and finish my PhD education.

Much thank to my vice supervisor, Dr. Kazuyoshi Kanamori, for his suggestion and help on my research and my Japanese.

Thank to Dr. Kei Morisato for the experimental support.

Special thanks to Ms. Sumiko Tsujikawa and Ms. Hiromi Kato for secretarial and daily support.

Special thanks to our group members, Mr. Ryoto Ueoka, Mr. Sato Yuji, Mr. Takayuki Kakegawa, Mr. Yosuke Hara, Mr. Shota Makimoto, Mr. Masayuki Kurita, Mr. Yuki Nakanishi, Mr. Rikuo Shigetake leave with many good memories.

Special thanks to Professor Dr. Lei Miao for giving two chances those changed my life. Without her, I cannot have such wonderful experience in Japan in the past three years.

Finally, I would like to thanks my parents, Mr. Jun Lu and Mrs. Sha Zhu for their upbringing and selfless support, and raising me up to see the beautiful world. Without them, I cannot obtain anything I have now.